Journal of Fluids and Structures (1997) **11,** 627–663

MOVING SURFACE BOUNDARY-LAYER CONTROL: A REVIEW

V. J. MODI
Department of Mechanical Engineering, The University of British Columbia Vancouver, B.C., Canada V6T 1Z4

(Received 22 September 1995 and in finally revised form 13 March 1997)

The paper briefly reviews developments in the exciting field of the moving surface boundary-layer control (MSBC). To begin with, application of the concept to a family of two-dimensional airfoils, investigated experimentally, is briefly summarized. The moving surface was provided by rotating cylinders located at the leading edge and/or trailing edge as well as the top surface of the airfoil. Results suggest that the concept is quite promising, leading to a substantial increase in lift and a delay in stall. Depending on the performance desired, appropriate combinations of cylinder location and speed can be selected to obtain favourable results over a wide range of the angle of attack. Next, the effectiveness of the concept in reducing drag of bluff bodies such as a two-dimensional flat plate at large angles of attack, rectangular prisms, and three-dimensional models of trucks is assessed. Results show that injection of momentum through moving surfaces, achieved here by introduction of bearing-mounted, motor-driven, hollow cylinders, can significantly delay separation of the boundary layer and reduce the pressure drag. The momentum injection procedure also proves effective in arresting wind-induced vortex resonance and galloping type of instabilities, suggesting possible application in the next generation of civil engineering structures. Now the attention is directed towards the role of computational fluid mechanics to this class of problems. The system performance, as predicted by results obtained using two distinctly different numerical procedures, shows good correlation with the wind tunnel data. Finally, results of a flow visualization study, conducted in a closed-circuit water tunnel using slit lighting and polyvinyl chloride tracer particles, are touched upon. They show, rather dramatically, the effectiveness of the MSBC.

1. INTRODUCTION

EVER since the introduction of the boundary-layer concept by Prandtl, there has been a constant challenge faced by scientists and engineers to minimize its adverse effects and control it to advantage. Methods such as suction, blowing, vortex generators, turbulence promoters, etc. have been investigated at length and employed in practice with a varying degree of success. A vast body of literature accumulated over years has been reviewed rather effectively by several authors including Goldstein (1938), Lachmann (1961), Rosenhead (1966), Schlichting (1968), Chang (1970) and others. However, the use of a moving wall for boundary-layer control has received relatively little attention. This is indeed surprising, as the Associate Committee on Aerodynamics, appointed by the National Research Council (1966), specifically recommended more attention in this area almost three decades ago.

Irrespective of the method used, the main objective of a control procedure is to prevent, or at least delay, the separation of the boundary layer from the wall. A moving surface attempts to accomplish this in two ways: it prevents the initial growth of the

0889–9746/97/060627 + 37 $25.00/fl970098

boundary layer by minimizing relative motion between the surface and the free stream; and it injects momentum into the existing boundary layer.

Newton was probably the first one to observe the effect of moving wall boundary-layer control on the trajectory of a spinning ball (Thwaites 1960), although the basis of the effect was not fully recognized. Almost 200 years later, Magnus (1853) studied lift generated by circulation and utilized the effect to construct a ship with a vertical rotating cylinder replacing the sail. Swanson (1961) and Iverson (1972) have presented excellent reviews of the literature on the Magnus effect. As early as in 1910, Prandtl himself demonstrated his ship of zero resistance through flow around two counter-rotating cylinders (Betz 1961), while Flettner (1925) applied the principle to ship propulsion in 1924 when he fitted large vertical rotating cylinders on the deck of the ''Buchau''. A little later, Goldstein (1938) illustrated the principle of boundary-layer control using a rotating cylinder at the leading edge of a flat plate. However, the most practical application of a moving wall for boundary-layer control was demonstrated by Favre (1938). Using an airfoil with the upper surface formed by a belt moving over two rollers, he was able to delay separation until the angle of attack (α) reached 55°, where the maximum lift coefficient of 3·5 was realized.

After a lull of more than twenty years (1938–1960), during which the tempo of research activity, as indicated by important contributions in the field, remained dormant, there were some signs of renewed interest in this form of boundary-layer control. Alvarez-Calderon & Arnold (1961) carried out tests on a rotating cylinder flap to evolve a high lift airfoil for STOL-type aircraft. The system was flight-tested on a single-engine, high-wing research aircraft designed by the Aeronautics Division of the Universidad Nacional de Ingenieria in Lima, Peru (Brown 1964). Around the same time, Brooks (1963) presented his preliminary results of tests on a hydrofoil with a rotating cylinder at the leading or trailing edge. For the leading-edge configuration only a small increase in lift was observed; however, for the latter case a substantial gain in lift resulted. Motivation for the test programme was to assess improvement in the fin performance for torpedo control. Along the same line, Steele & Harding (1970) studied the application of rotating cylinders to improve ship maneuverability. Extensive force measurements and flow visualization experiments were conducted using a water tunnel and a large circulating water channel. Three different configurations of rudder were used, with the rotating cylinder: (i) in isolation; (ii) at the leading edge of a rudder; and (iii) combined with a flap-rudder, the cylinder being at the leading edge of the flap.

From the overall consideration of hydrodynamic performance, mechanical complexity and power consumption, the configuration in (ii) was preferred. An application to a 250 000-ton tanker showed the power requirement for a cylinder 1 m in diameter rotating at 350 rpm to be around 400 kW.

Of some interest is the North American Rockwell's OV-10A, which was flight-tested by NASA's Ames Research Center (Cichy *et al.* 1972; Weiberg *et al.* 1973; Cook *et al.* 1974). Cylinders, located at the leading edge of the flaps, were made to rotate at a high speed with the flaps in lowered position. The main objective of the test programme was to assess handling qualities of the propeller-powered STOL-type aircraft at high lift coefficients. The aircraft was flown at speeds of 29–31 m/s, along approaches up to $-8°$, which corresponded to a lift coefficient of about 4·3. In the pilot's opinion, any further reductions in the approach speed were limited by the lateral-directional stability and control characteristics. Excellent photographs of the airplane on ground (showing the cylinders in position) and in flight have been published in the Aviation Week and Space Technology (Hotz 1971).

Around the same time, Tennant (1971, 1973) presented an interesting analysis for

the two-dimensional moving wall diffuser with a step change in area. The diffuser incorporated rotating cylinders to form a part of its wall at the station of the area change. Preliminary experiments were also conducted for the area ratio up to 1:2·5, which showed no separation for appropriate moving surface to diffuser inlet velocity ratio. Johnson *et al.* (1975) have also conducted tests with a wedge-shaped flap having a rotating cylinder as the leading edge. Flap deflection was limited to 15° and the critical cylinder velocity necessary to suppress separation was determined. Effects of increase in gap size (between the cylinder and the flap surface) were also assessed. No effort was made to observe the influence of an increase in cylinder surface velocity beyond $U_c/U = 1{\cdot}2$ (U_c = cylinder surface velocity, U = freestream velocity). Subsequently, Tennant *et al.* (1976) have reported circulation control for a symmetrical airfoil with a rotating cylinder forming its trailing edge. For zero angle of attack, the lift coefficient (C_L) of 1·2 was attained with $U_c/U = 3$. Also of interest is their study (Tennant *et al.* 1977, 1978) concerning the boundary-layer growth on moving surfaces accounting for gap effects.

This was the state of the development when the author entered the field. The subsequent contributions to the literature are essentially from his group, which undertook a planned, comprehensive investigation involving:

(i) wind tunnel tests with a family of two-dimensional airfoils as well as two- and three-dimensional bluff bodies;
(ii) numerical simulations; and
(iii) flow visualization studies.

Mostly, these studies were conducted in the subcritical range of $4{\cdot}0 \times 10^4$–10×10^4, where the Reynolds number effects are relatively insignificant. This facilitated comparison of experimental, numerical and flow visualization results. As can be expected, the amount of information obtained through planned variations of the important parameters is literally enormous. Here these developmens are briefly reviewed, touching upon the methodologies used and sets of typical results useful in establishing trends.

2. TWO-DIMENSIONAL AIRFOILS WITH THE MSBC

2.1. Wind Tunnel Test-Program

Figure 1 shows a family of two-dimensional airfoils with different positions of the rotating elements used to inject momentum. Geometry of the airfoil (thickness ratio, camber, etc.) were also varied. To provide flexibility in locating the cylinder on the airfoil and permit testing of multi-cylinder configurations, a sectional design was adopted. The rotating cylinders were mounted between high-speed bearings housed in the brackets at either end of the model. They were driven by $\frac{1}{4}$ h.p. 3·8 A variable-speed motors, located outside the tunnel, through standard couplings (Figure 2).

Typically, a model was provided with a total of 44 pressure taps, distributed over the circumference, to yield detailed information about the surface loading with an accuracy of $6{\cdot}9 \times 10^{-2}$ N/m^2. Approximately 0·38 m along the chord and 0·68 m long, it spanned the tunnel test-section, $0{\cdot}91 \times 0{\cdot}68 \times 2{\cdot}6$ m, to create essentially two-dimensional flow

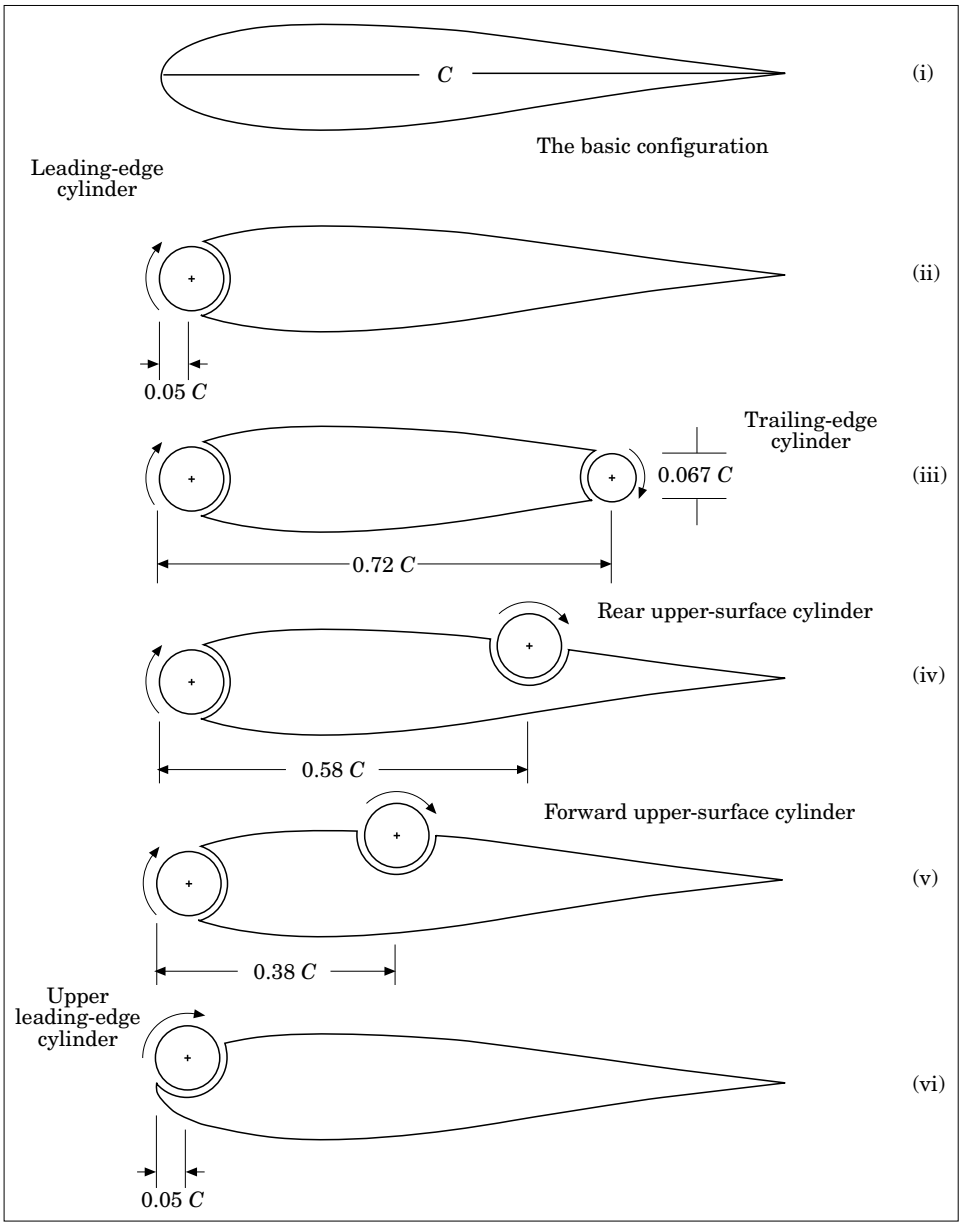

Figure 1. Various rotating-cylinder configurations studied with the Joukowsky airfoil model.

conditions. It was supported by an Aerolab six-component strain gauge balance (resolution 10^{-3} N) and tested in a low-speed, low-turbulence return-type wind tunnel, where the airspeed can be varied from 1 to 50 m/s with a turbulence level of less than 0·1% (Modi *et al.* 1981, 1987).

The tests were conducted over an extended range of the angle of attack α and cylinder rotational speeds, corresponding to $U_c/U = 0$–4, at a Reynolds number (Re, based on U and the chord) of $4{\cdot}62 \times 10^4$. The choice of the Reynolds number in this case was dictated by vibiration problems with multi-cylinder configurations operating

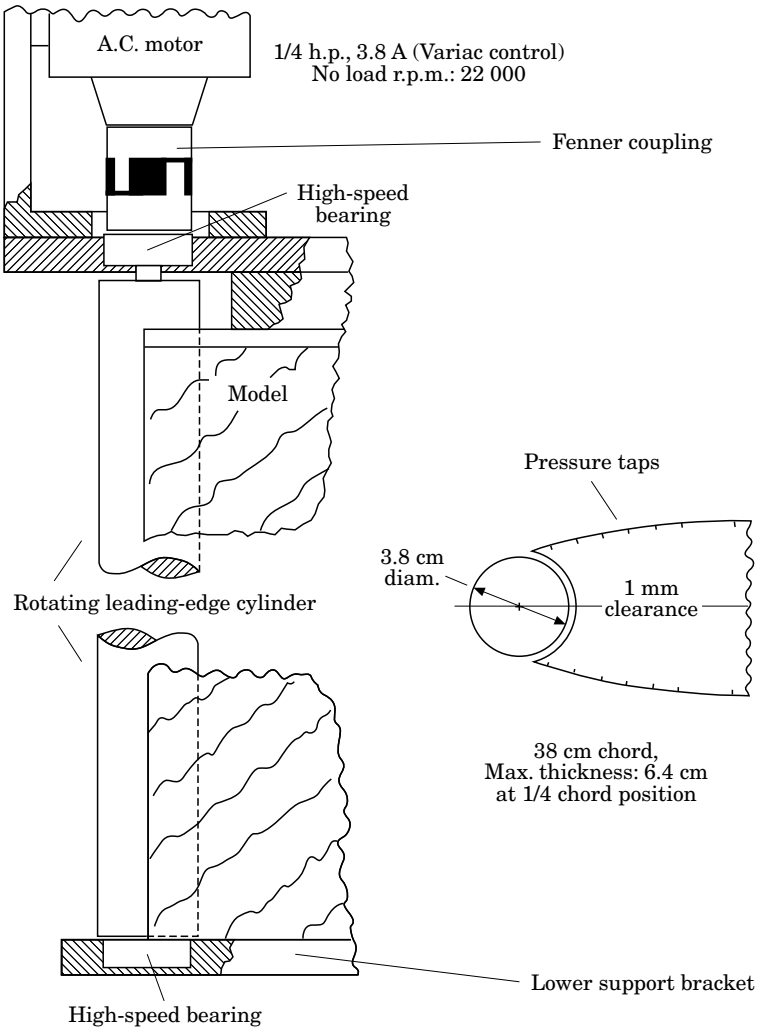

Figure 2. Detailed schematic of the leading-edge rotating cylinder and cylinder-drive mechanism.

at high rotating speeds (around 8000 r.p.m. for $U_c/U = 4$). The pressure plots were integrated in each case to obtain the aerodynamic coefficients. The coefficients were also measured independently using the Aerolab balance to assess two-dimensional character of the flow.

The relatively large angles of attack used in the experiments result in a considerable blockage of the wind-tunnel test-section, from 21% at $\alpha = 30°$ to 30% at $\alpha = 45°$. The wall confinement leads to an increase in local wind speed at the location of the model, thus resulting in an increase in aerodynamic forces. Several approximate correction procedures have been reported in the literature to account for this effect. However, these procedures are mostly applicable to streamlined bodies with attached flow. A satisfactory procedure applicable to a bluff body offering a large blockage in a flow with separating shear layers is still not available.

With rotation of the cylinder(s), the problem is further complicated. As shown by the pressure data and confirmed by flow visualization, the unsteady flow can be separating and reattaching over a large portion of the top surface. In the absence of any

reliable procedure to account for wall confinement effects in the present situation, the results are purposely presented in the uncorrected form, unless specified otherwise.

2.2. Base Airfoil

The pressure distribution data for the base airfoil (i.e. in the absence of the modifications imposed by the leading-edge or upper-surface cylinder) are presented in Figure 3. Here X represents the coordinate along the chord and C is the chord length. The leading edge was now formed by a snugly fitting plug (the nose fill-in section). Due to the practical difficulty in locating pressure taps in the cusp region, there is an apparent

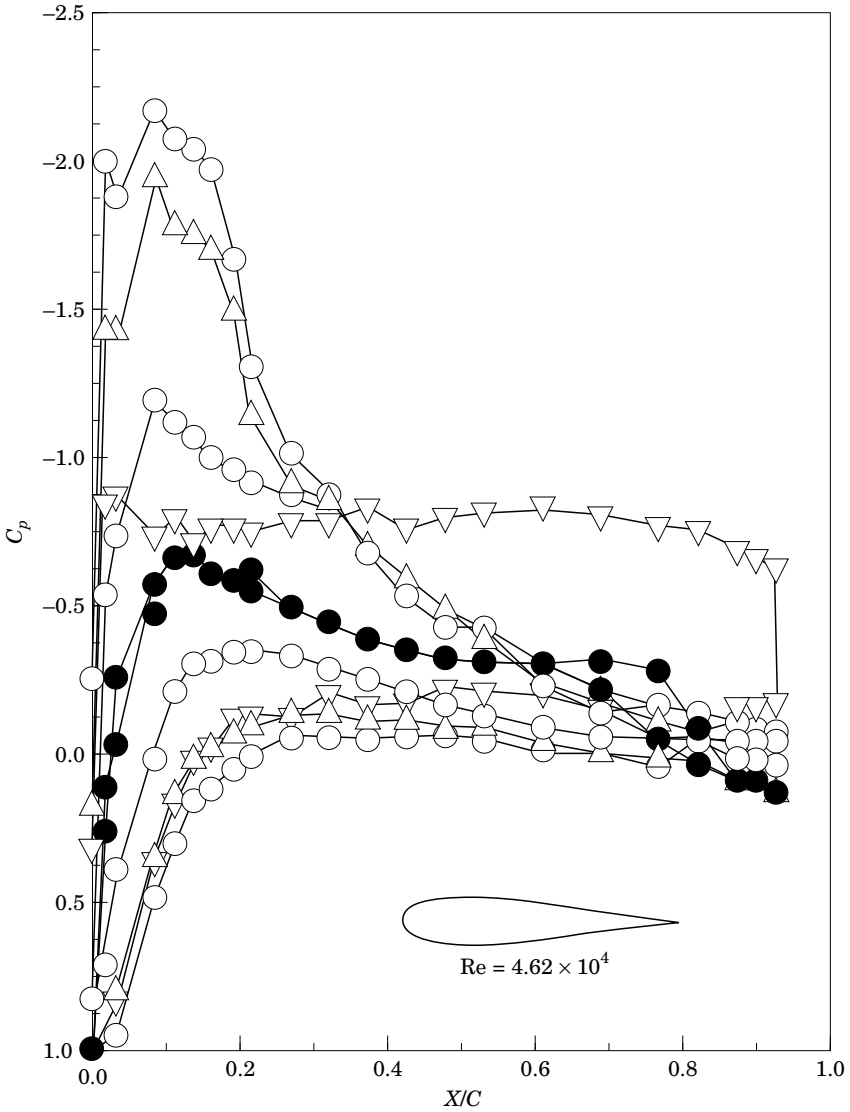

Figure 3. Experimentally obtained pressure distribution plots for the basic Joukowsky model. (●) $\alpha = 0°$; (○) $\alpha = 4°$; (△) $\alpha = 8°$; (◯) $\alpha = 10°$; (▽) $\alpha = 12°$.

discontinuity in the pressure plots near the trailing edge. However, this region has little importance in the present discussion. It is apparent that the airfoil, in the absence of any modifications to its nose geometry, stalls at an angle of attack of around 10°–12°. The results serve as a reference to assess the effect of rotating cylinders at different locations.

2.3. Leading Edge Cylinder

Figure 4 summarizes the effects of modification of the airfoil with the leading-edge cylinder and cylinder rotation. The base airfoil has a maximum lift coefficient of about

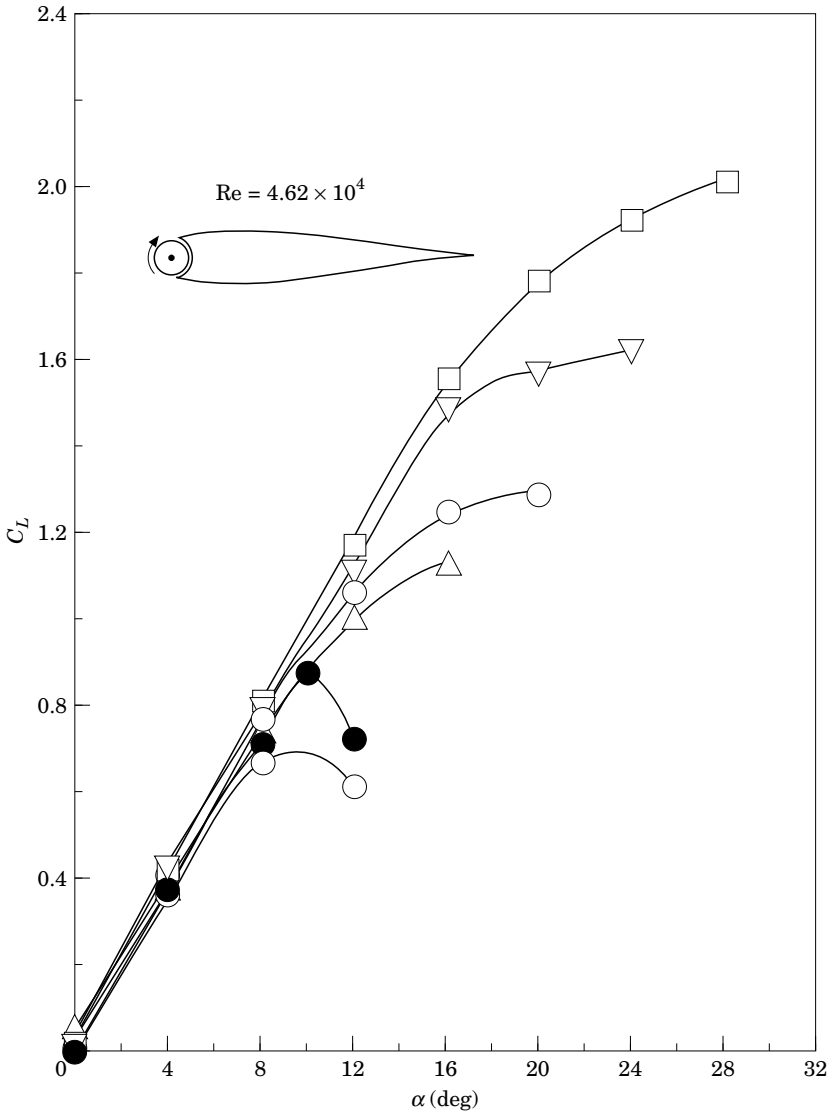

Figure 4. Effect of the leading-edge cylinder rotation on the lift and stall characteristics of the Joukowsky model. (●) Base airfoil; (○) $(U_C/U)_{\text{l.e.}} = 0$; (△) $(U_C/U)_{\text{l.e.}} = 1$; (◯) $(U_C/U)_{\text{l.e.}} = 2$; (▽) $(U_C/U)_{\text{l.e.}} = 3$; (□) $(U_C/U)_{\text{l.e.}} = 4$.

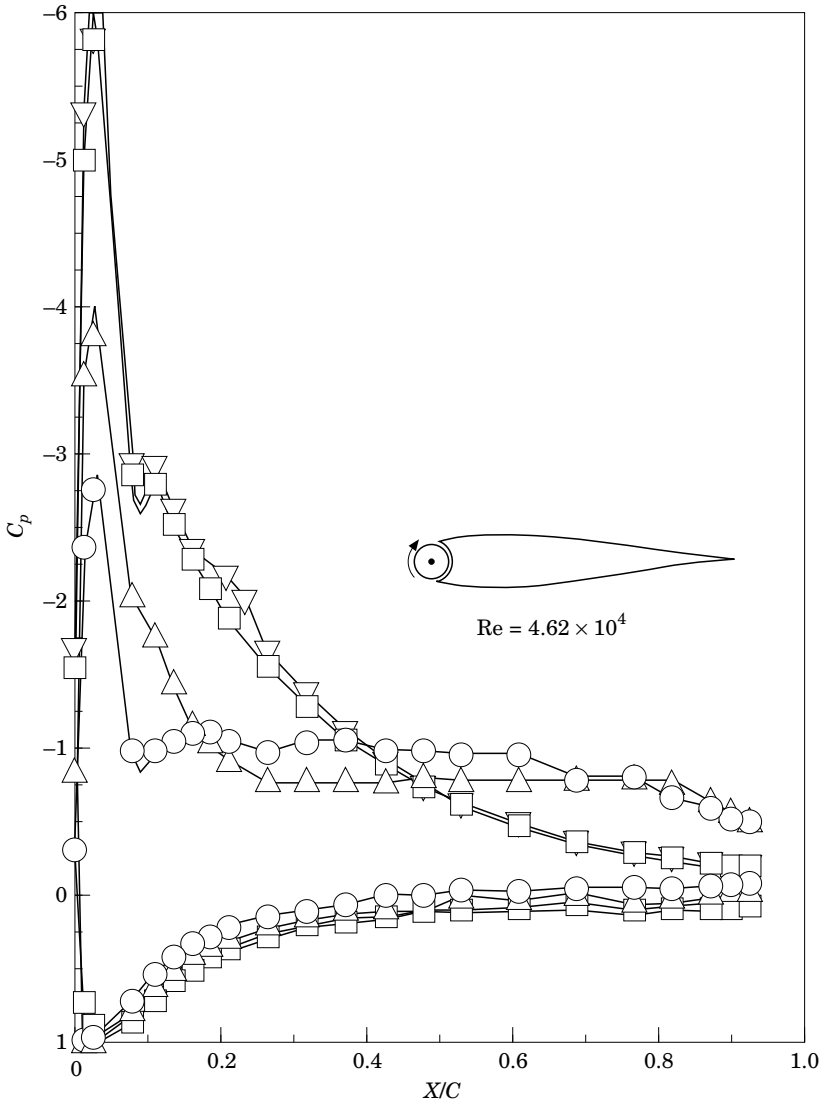

Figure 5. Effect of increasing the rate of cylinder rotation on pressure distribution around the model at a relatively larger angle of attack of $\alpha = 16°$. (○) $U_C/U = 1$; (△) $U_C/U = 2$; (□) $U_C/U = 3$; (▽) $U_C/U = 4$.

0·88 at an angle of attack of 10°. There is a penalty associated with the modified nose geometry as well as due to the gap, but even at the lowest rate of rotation of the cylinder ($U_c/U = 1$) the lift and stall characteristics are significantly improved. The airfoil exhibits a desirable flattening of the lift curve at stall. The maximum lift coefficient measured with $U_c/U = 4$ was around 2 at $\alpha = 28°$, which is more than twice the lift coefficient of the base airfoil.

Typical pressure plots at a relatively larger angle of attack are presented in Figure 5 to assist in more careful examination of the local flowfield. As the angle of attack of the airfoil is increased, the flow starts to separate from the upper surface close to the leading edge. At $\alpha = 16°$, for example, the cylinder rotating at $U_c/U = 1$ only keeps the flow attached at the leading edge. However, as the rate of rotation is increased, the size of the separated region is reduced, and at the higher rates of rotation the flow is

again completely attached. Note that the point of separation on the upper surface clearly moves downstream with an increasing rate of rotation. The flow separates at around $X/C = 25\%$ with $U_c/U = 2$, around $X/C = 80\%$ when U_c/U is increased to 3, and at the trailing edge with the highest U_c/U used. The flow visualization study discussed later substantiated this general behaviour rather dramatically.

2.4. Comparative Performance

As indicated in Figure 1, besides the leading edge cylinder (l.e.), the configurations tested include the trailing edge cylinder (t.e.), forward upper-surface cylinder (f), rear upper-surface cylinder (r), leading edge and upper surface cylinders (l.e.r., l.e.f.,respectively), and upper leading-edge cylinder (u.l.e.). This resulted in a vast amount of information (Mokhtarian 1988; Mokhtarian & Modi 1988; Mokhtarian *et al.* 1988, Modi *et al.* 1991a). It would be helpful to compare distinctive features of the different configurations to establish their relative merits. Figure 6 attempts to achieve this objective. Results of the standard Joukowsky airfoil (symmetrical, 15% thickness), with its $C_{L\max} = 0{\cdot}88$ and $\alpha_{\text{stall}} = 10°$, serve as reference for all the cases presented.

The leading-edge cylinder is quite effective in extending the lift curve, without significantly changing its slope, thus substantially increasing the maximum lift coefficient ($\approx$2) and delaying the stall angle (28°). Further improvements in the maximum lift coefficient and stall angle are possible when the leading-edge cylinder is used in conjunction with an upper surface cylinder. This configuration also results in a lower drag, due to a large recovery of pressure near the trailing edge, at moderately high angles of attack. The $C_{L\max}$ realized with the leading-edge and forward upper-surface cylinder was about 2·73 ($\alpha = 36°$), approximately three times that of the base configuration.

A rotating cylinder on the upper side of the leading edge (u.l.e.) also proves very effective. Although the maximum coefficient of lift realized with its rotation is slightly lower ($\approx$2·35), it does have a major advantage in terms of mechanical simplicity. Note that now the lift curve has a lower slope and is not an extension of the base airfoil lift curve. Hence, the lift at a given α is relatively lower; however, the stall is delayed to around 48°.

On the other hand, to improve the lift over the range of low to medium angles of attack ($\alpha \leq 20°$), the trailing-edge cylinder proves much more effective, particularly in conjunction with the leading-edge cylinder. The suction over the airfoil upper surface as well as the compression on the lower surface are increased dramatically, with a higher rate of rotation of this cylinder, resulting in a substantial increase in lift ($\approx$195%).

Thus, depending on the intended objective in terms of the desired $C_{L\max}$ and stall angle, one can select an appropriate configuration to initiate a preliminary design.

One would like to assess relative merit of the moving surface boundary-layer control with the other procedures for generating high lift, such as blowing, suction, etc. Obviously, to be useful, such a comparison has to be based on well planned experiments conducted under controlled and comparable conditions, as otherwise it can lead to misleading conclusions. Unfortunately, such results permitting rational comparison have not been recorded in the literature. However, it is possible to make a few general observations.

Beside its striking success in increasing the lift and delaying stall, one of the attractive features of the moving surface boundary-layer control is the negligible amount of power involved in driving the cylinders. Essentially it corresponds to the

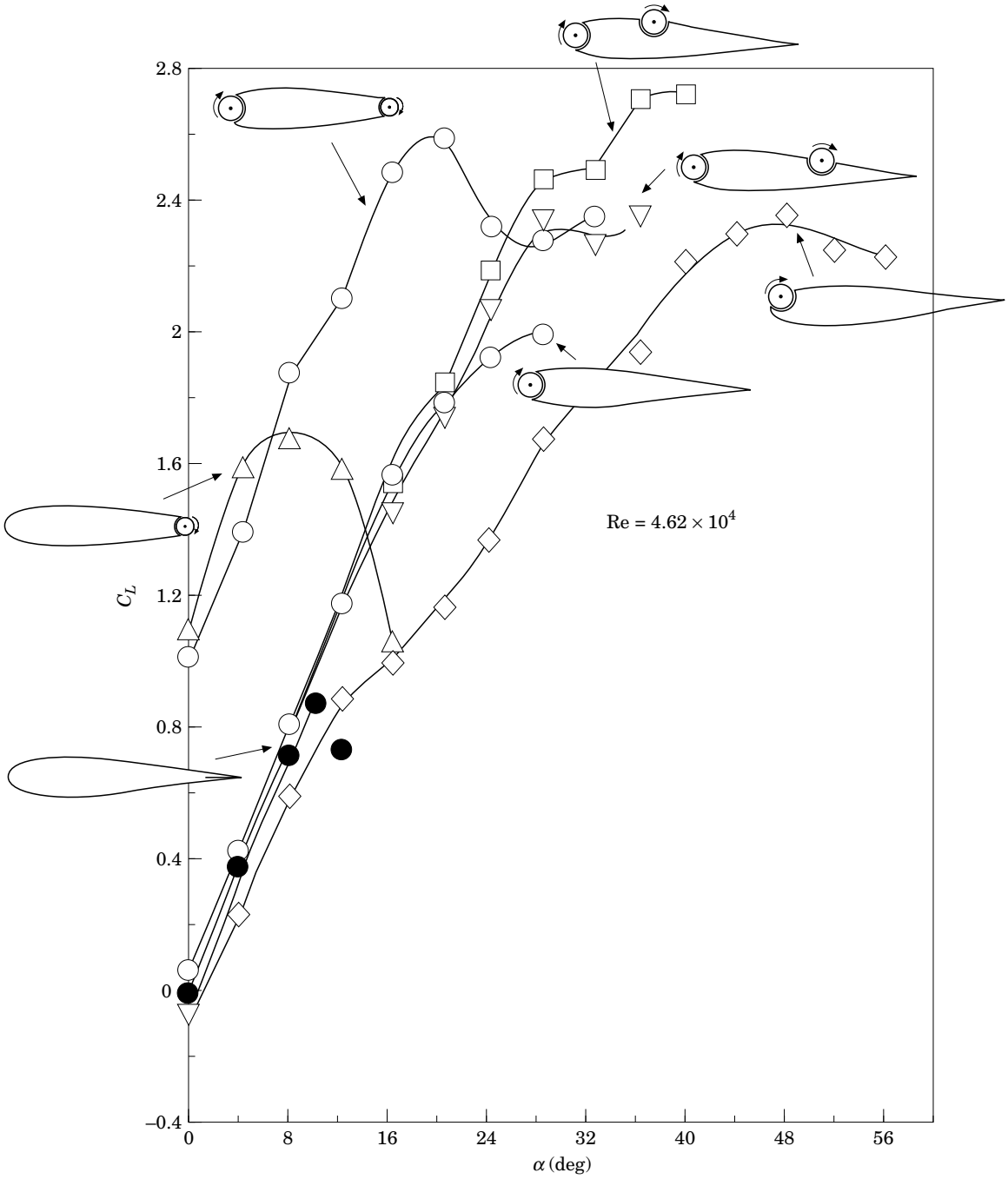

Figure 6. Plots to assess relative influence of different conflgurations studied on the lift and stall characteristics. (●) Base airfoil; (○) $(U_C/U)_{\text{l.e.}} = 4$; (△) $(U_C/U)_{\text{t.e.}} = 4$; (◯) $(U_C/U)_{\text{l.e.}}$, $(U_C/U)_{\text{t.e.}} = 4$; (▽) $(U_C/U)_{\text{l.e.}}$, $(U_C/U)_{\text{r}} = 4$; (□) $(U_C/U)_{\text{l.e.}}$, $(U_C/U)_{\text{f}} = 4$; (◇) $(U_C/U)_{\text{u.l.e.}} = 4$.

bearing friction and the torque contributed by forces on the surface of the cylinder. Note, the cylinder itself can be hollow, thus minimizing the inertia effect. The $\frac{1}{4}$ h.p. motor used in the present study was much larger than necessary. It was used because

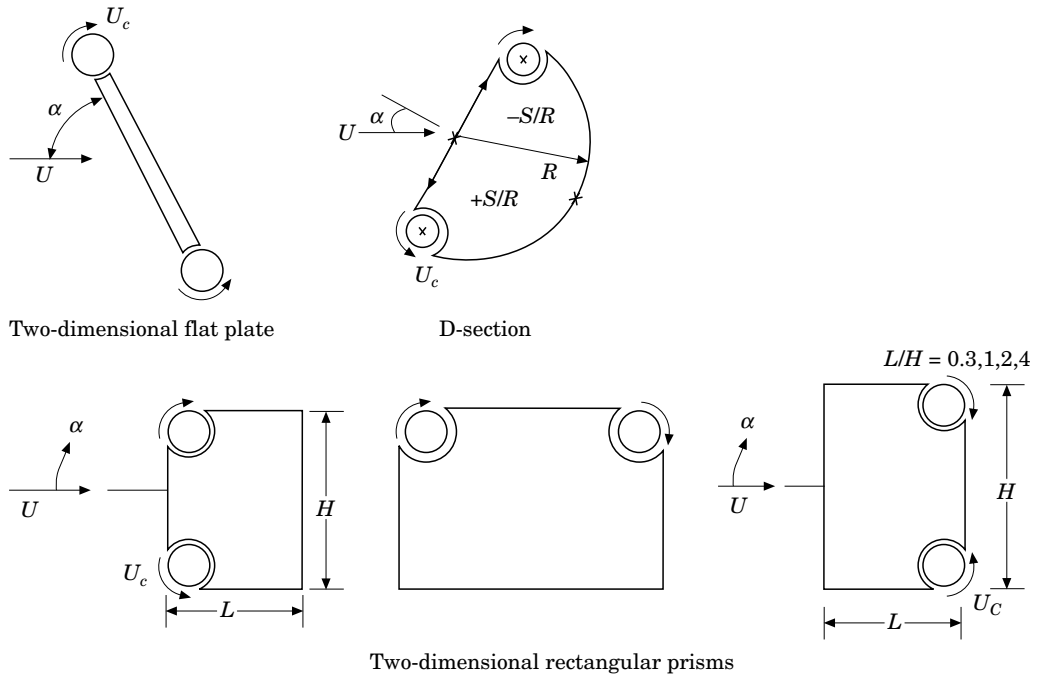

Figure 7. Schematic diagrams of the two-dimensional bluff bodies used during the wind tunnel tests.

of availability. Even a $\frac{1}{16}$ h.p. motor would have served the purpose. Thus the power required is virtually insignificant compared to active blowing or suction for boundary-layer control, where the power consumption is likely to be considerably larger.

3. FLAT PLATE, RECTANGULAR PRISMS AND D-SECTION

Next the attention was turned to bluff geometries, where a reduction in the drag is of more importance than the increase in lift. Schematic diagrams of some of the configurations considered for the study are indicated in Figure 7. They include a two-dimensional flat plate, a D-section, as well as two- and three-dimensional prisms with cylinders for the MSBC. Details of the test arrangement and results are discussed at length in publications by Modi (1991), Modi *et al.* (1991b, c, d, e, 1992), Ying (1991), Kubo *et al.* (1992) and Munshi *et al.* (1995).

Tests with the flat plate were carried out with either of the cylinders rotating independently; or with the two cylinders rotating together but in the opposite sense, for effective momentum injection to assist in the boundary-layer control. Both the lift as well as the drag results showed remarkable improvement (Modi *et al.* 1991e).

Of course, the maximum reduction in the wake, and hence the corresponding decrease in the presure drag coefficient, can be expected when both cylinders are rotating, as shown in Figure 8 (Modi *et al.* 1991c). For $\alpha = 90°$, a decrease in the drag coefficient from 1·85 at $U_c/U = 0$ to 0·47 at $U_c/U = 3$ represents a reduction of around 75%. The flow visualization photographs also showed a remarkable reduction in the wake width, thus qualitatively substantiating the trend suggested by the wind tunnel test results.

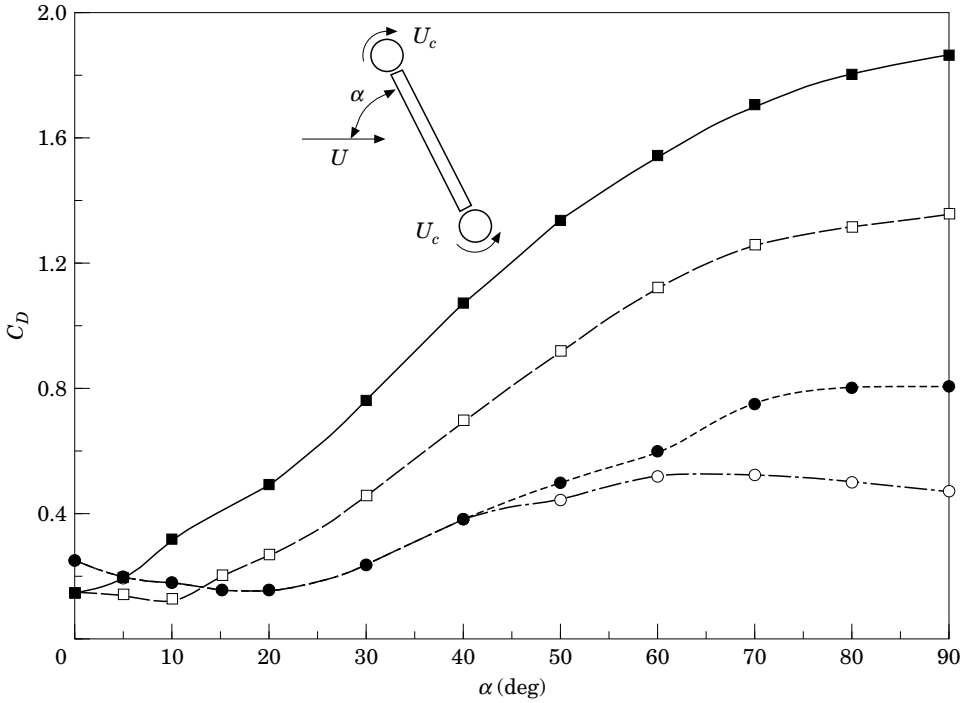

Figure 8. Plots showing significant reduction in drag of a two-dimensional flat plate with the moving surface boundary-layer control applied at both the leading and trailing edges. Note, at $\alpha = 90°$, a reduction in C_D is around 75%. (■) $U_C/U = 0$; (□) $U_C/U = 1$; (●) $U_C/U = 2$; (○) $U_C/U = 3$.

Rectangular prisms with rotating cylinders at two adjacent corners provide three basic configurations for study: the side with cylinders facing the flow, forming the top face, or representing the rear face. Various intermediate configurations can be obtained by systematically changing the angle of attack. With four values of L/H, to help assess the effect of boundary-layer reattachment and reseparation further downstream, and four values of U_c/U, the amount of information obtained is rather extensive (Modi *et al.* 1991c, d, e, 1992). Only some representative results are touched upon here.

Figure 9 shows a sample of results for the experimental phase where the rotating elements are on the top surface, i.e. parallel to the free-stream for $\alpha = 0$. Cases corresponding to single- and two-cylinder rotation for the square prism model are considered. At the outset it is apparent that rotation of the second cylinder has very little effect on the flow field for $\alpha > 5°$, and hence on C_D, as now the trailing edge cylinder lies in the wake. However, for smaller and negative α, it is quite successful in further reducing C_D: from 1·7 at $\alpha = 0°$ and $U_c/U = 3$ for the upstream cylinder rotation to 1·3 when both the cylinders are rotating. A reduction in the drag coefficient by 54% with both the cylinders rotating is indeed quite impressive.

The influence of rotating cylinders located on the rear vertical face of the square and rectangular prisms was also investigated. In this case, the boundary-layer separates at the top and bottom leading edges and the rotating cylinders are submerged in the wake, thus reducing their effectiveness. Now the reduction in C_D at $\alpha = 0°$ and $U_c/U = 3$ was found to be only 13% for the square prism and virtually zero for the rectangular prism, compared to 53% and 40%, respectively, for the case with cylinders at the front face.

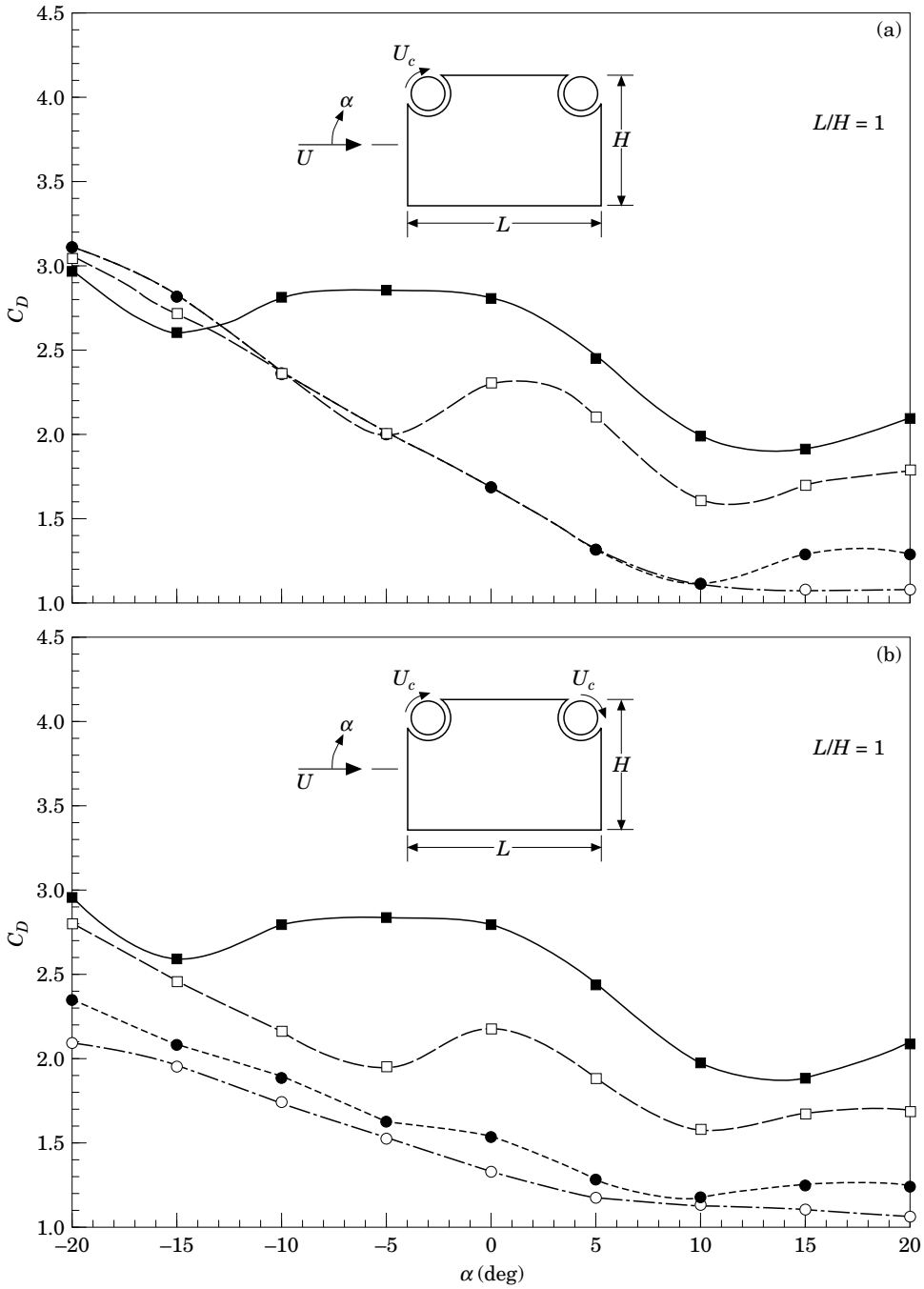

Figure 9. Variation of drag coefficient with the angle of attack for a two-dimensional square prism when the boundary-layer control is applied at the top surface. (a) A rotating cylinder at the leading edge; (b) rotating cylinders at leading and trailing edges. (■) $U_C/U = 0$; (□) $U_C/U = 1$; (●) $U_C/U = 2$; (○) $U_C/U = 3$.

A word about the fluid dynamics of D-section in the presence of MSBC would be appropriate, as it represents transition in bluffness from the airfoil to the family of rectangular prisms (Munshi *et al.* 1995). The mean static pressure distribution around the D-section was measured by a 48-channel Scanivalve pressure transducer connected to a computerized data acquisition system. Figure 10 shows the pressure distribution at several angles of attack (α) with cylinders stationary ($U_c/U = 0$) as well as rotating ($U_c/U =$ 2 and 4). At $\alpha = 0$ and in the absence of the cylinder rotation, the flow separates near the corners of the D-section, as evident from the pressure distribution. The pressure coefficient (C_p) in the wake is negative, resulting in a large drag force. As the cylinder rotation speed is increased from zero to a maximum ($U_c/U = 4$), large suction peaks appear at the rotating cylinders (i.e. the frontal position of the D-section) and the negative wake pressure experiences a significant positive change. Also, note that the point of separation has moved considerably downstream. Overall, a net reduction in the drag of around 42% was observed. As the angle of attack is increased from zero, the symmetry in the pressure distribution is disrupted and the stagnation point starts to move towards the upstream rotating cylinder. The suction peaks at the rotating cylinders progressively become smaller as the angle of attack increases. At $\alpha \approx 60°$ the stagnation point is located very close to the upstream corner. This situation suggests that the direction of the upstream rotating cylinder should now be reversed for the MSBC to be effective. Further increase in the angle of attack beyond 60°, without reversing the cylinder rotation, shows that the benefits of the MSBC are lost ($\alpha = 90°$). In fact, as can be expected, the wrong direction of the momentum injection led to an increase in drag at $\alpha = 105°$.

4. TRACTOR-TRAILER TRUCK CONFIGURATION

4.1. Background

A comprehensive literature review of road-vehicle aerodynamics suggests that, although aerodynamically contoured car design has become a standard practice lately, the trucks and buses have changed little during the past 30 years (Sovaran *et al.* 1978; Kramer & Gerhardt 1980). Most of the modifications have been limited to rounded edges with provision for vanes, skirts and flow deflectors. The benefit due to some of the add-on devices is still a matter of controversy and, at best, marginal under conditions other than the specific ones used in their designs. Bearman (1980) has presented an excellent review on the subject (with 54 references cited). The thesis by Wacker (1985) also discusses the limited influence of add-on devices, with a possibility of increasing the drag under non-optimal conditions. On the other hand, it was found that judicious choice of ground clearance, gap size between the tractor and trailer, and back inclination can reduce the drag coefficient by a significant amount.

4.2. Model and Test Procedure

A $\frac{1}{12}$ scale tractor-trailer truck model was constructed out of Plexiglas. The model has a trailer with width $B = 22{\cdot}7$ cm, height $H = 26{\cdot}2$ cm, length $L = 128{\cdot}4$ cm, and a hydraulic diameter of 0·311 m. A typical truck model was supported by four steel guy wires which were suspended from the ceiling and carried turnbuckles to help level the

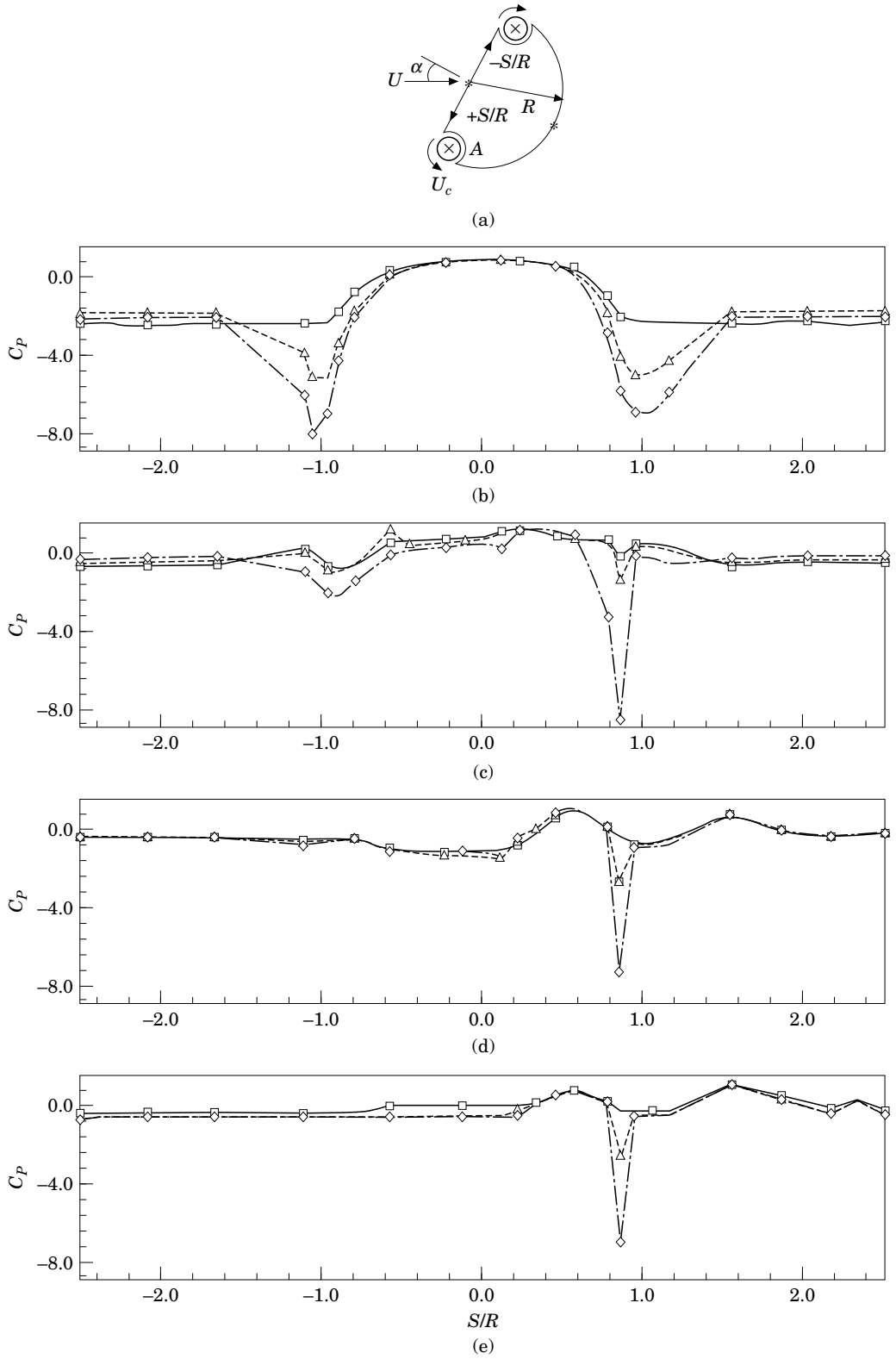

Figure 10. Pressure plots for the D-section showing effects of the angle of attack and momentum injection. (a) $\alpha = 0°$; (b) $\alpha = 60°$; (c) $\alpha = 90°$; (d) $\alpha = 105°$, Re = 66 000, (□) $U_C/U = 0$ (△) $U_C/U = 2$, (◇) $U_C/U = 4$.

model. As the length of the wire (≈145 cm) is much larger than the maximum horizontal displacement of the truck model (≤5 cm), the drag-induced displacement was essentially linear in the downstream direction.

Variation in the drag due to the boundary-layer control devices being rleatively small required development of a sensitive transducer for its measurement. The drag-induced downstream motion of the model was transmitted by an inelastic string to a cantilever beam with a pair of strain gauges near its root. The gauges formed a part of the Wheatstone Bridge (i.e. the *Bridge Amplifier Meter,* BAM) and the amplified filtered output was recorded using a DISA voltmeter. The sensitivity of the drag measurements was around 0·4 gm/mV.

4.3. Results and Discussion

Tests with a scale model of the truck were carried out in the boundary-layer tunnel with negligible blockage effect (blockage ratio = 1·2%). The trailer was provided with rotating cylinders at its top leading edge and a downstream location. The L/H ratio for the trailer was approximately 3·75, which suggested that rotation of the rear cylinder will have virtually no effect on the drag reduction. The wind tunnel tests substantiated this observation. Considering the fact that (i) around 70% of goods in North America are transported by trucks, (ii) depending on the speed, approximtely 40–70% of the power is expended in overcoming the aerodynamic drag, (iii) on an average, a truck travels around 150 000 kg/year, even a 1% reduction in the drag coefficient can translate into a substantial saving in fuel cost.

In the beginning, to assess the role of the cylinder surface roughness on the efficiency of the momentum injection process, tests were carried out with three different rotating elements: cylinder with smooth surface; cylinder surface roughness of grade 80; and cylinder surface roughness of grade 40. In the absence of momentum injection, the truck drag coefficient was around 0·81 and reduced to 0·765 at $U_c/U = 2$ for the smooth cylinder case. The surface roughness of the cylinder improved the performance further, reducing C_D to around 0·73 at $U_C/U = 2$ for the roughness of grade 80. Increasing the surface roughness to 40 dropped the minimum C_D to 0·7, a reduction of around 13% (Modi *et al.* 1991d,e).

With the positive influence of the cylinder roughness on the momentum injection process and associated reduction in the drag, it seemed logical to introduce the momentum more directly. This was achieved in several ways:

(i) by providing increased cylinder surface roughness through machining helical grooves or splines running parallel to the cylinder axis;
(ii) by keeping one cylinder at the top leading edge of the trailer (referred to as the front cylinder) and locating the second cylinder (rear cylinder) at an optimum distance downstream; the objective is to inject additional momentum in the boundary layer to compensate for dissipation of the momentum introduced by the front cylinder, and thus counter the emergence of an adverse pressure gradient;
(iii) by raising the cylinders so as to immerse them in the boundary layer and assess the effect of cylinder orientation.

Extensive wind tunnel tests with different combinations of the speed ratio (U_c/U), cylinder location and surface roughness showed the helical groove and spline

TABLE 1

Wind-tunnel tests conducted with different speed ratios and orientation of the twin helical groove and spline cylinders. Location of the front cylinder is at the top leading edge of the trailer. The second cylinder is located 25·4 cm (10 in) downstream.

Cylinder location	Case								
	1	2	3	4	5	6	7	8	9
Front raised, mm	—	—	—	6·35	6·35	12·7	12·7	12·7	6·35
Rear raised, mm	—	6·35	12·7	12·7	—	—	6·35	12·7	6·35

geometry, with one cylinder located at the leading edge and the other 25·4 cm downstream, to be quite effective. The influence of raising the cylinder above the trailer surface was also found to be significant. The cylinder orientations studied with helical and spline roughnesses are indicated in Table 1. Figure 11 schematically shows the model and the test-arrangement. The considerable amount of information obtained has been reported by Modi *et al.* (1991d, e). Only some representative results are presented here to indicate the potential.

Figure 12(a) shows the effect of the spline cylinder rotation for case 1, i.e. when both the cylinders are flush with the top face of the trailer. U_{cf} and U_{cr} refer to front and rear cylinder surface speeds, respectively. At the outset it is apparent that the front cylinder rotation ($U_{cr} = 0$) reduces the drag coefficient rather significantly, from 1·14 at $U_{cf} = 0$ to 0·96 at $U_{cf}/U = 4{\cdot}1$, a drop of around 15·8%. Rotation of the rear cylinder improves the situation further, and for both the cylinder with a speed ratio $U_c/U = 4{\cdot}1$ the reduction in C_D reaches 22·8%!

The effect of raising the rear cylinder is shown in Figure 12(b). Note that, even in the absence of the momentum injection ($U_{cf} = U_{cr} = 0$), the reference drag coefficient is slightly reduced ($C_D = 1{\cdot}19$). This may be attributed to the combined effect of an increase in the projected area on which the drag coefficient is based and the large wake width caused by the rear cylinder. Rotation of the front cylinder does not seem to improve the situation significantly (compared to case 1); as for $U_{cf}/U = 4{\cdot}1$, a reduction in drag is 16·8%. With both the cylinders rotating at a speed ratio of 4·1, the decrease in drag coefficient amounts to 24·8%.

Essentially the same trend continued to persist when the front cylinder was also raised (case 7). The drag coefficient in the absence of the cylinder rotation dropped further to 1·12, as explained before. With $U_{cf}/U = U_{cr}/U = 4{\cdot}1$, the reduction in drag reached almost 26%. Thus the splined geometry of the rotating elements with raised positions appears quite promising in reducing the pressure drag of the tractor-trailer truck configuration through the MSBC.

5. NUMERICAL SIMULATIONS

Simulation of fluid dynamical problems has been classically approached in two fundamentally different ways: (a) modelling of the physical character of a phenomenon, as approached by Prandtl, through insight into the physics of the problem; (b) simulation of the governing equations of motion as accomplished through finite element or finite difference schemes. As can be expected, each has its advantages and limitations. Here the effectiveness of both procedures is illustrated in the study of the complex problem of a multi-element airfoil with momentum injection using:

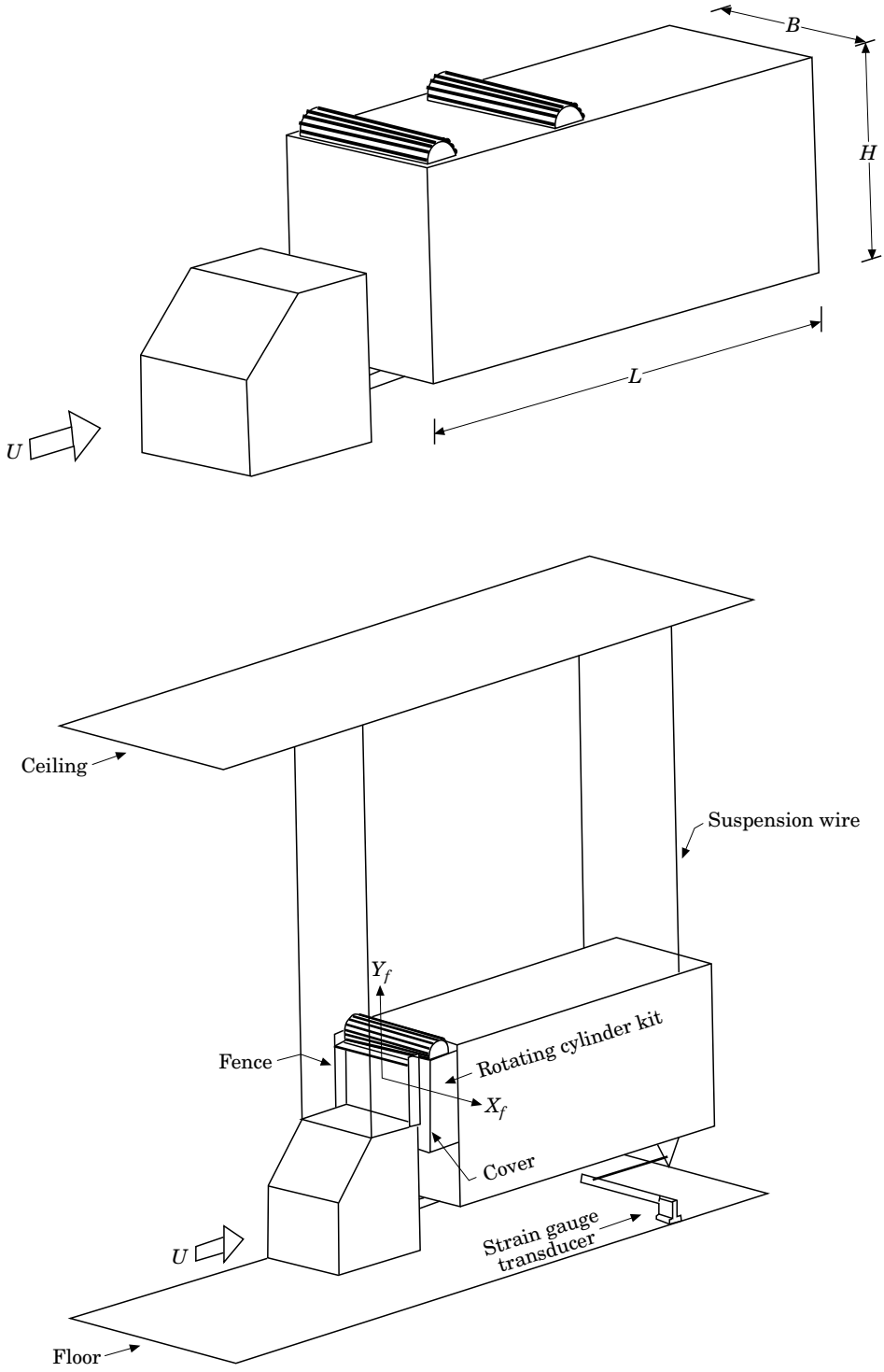

Figure 11. A schematic diagram of the 3-D tractor-trailer truck model and its test arrangement in the boundary-layer wind tunnel.

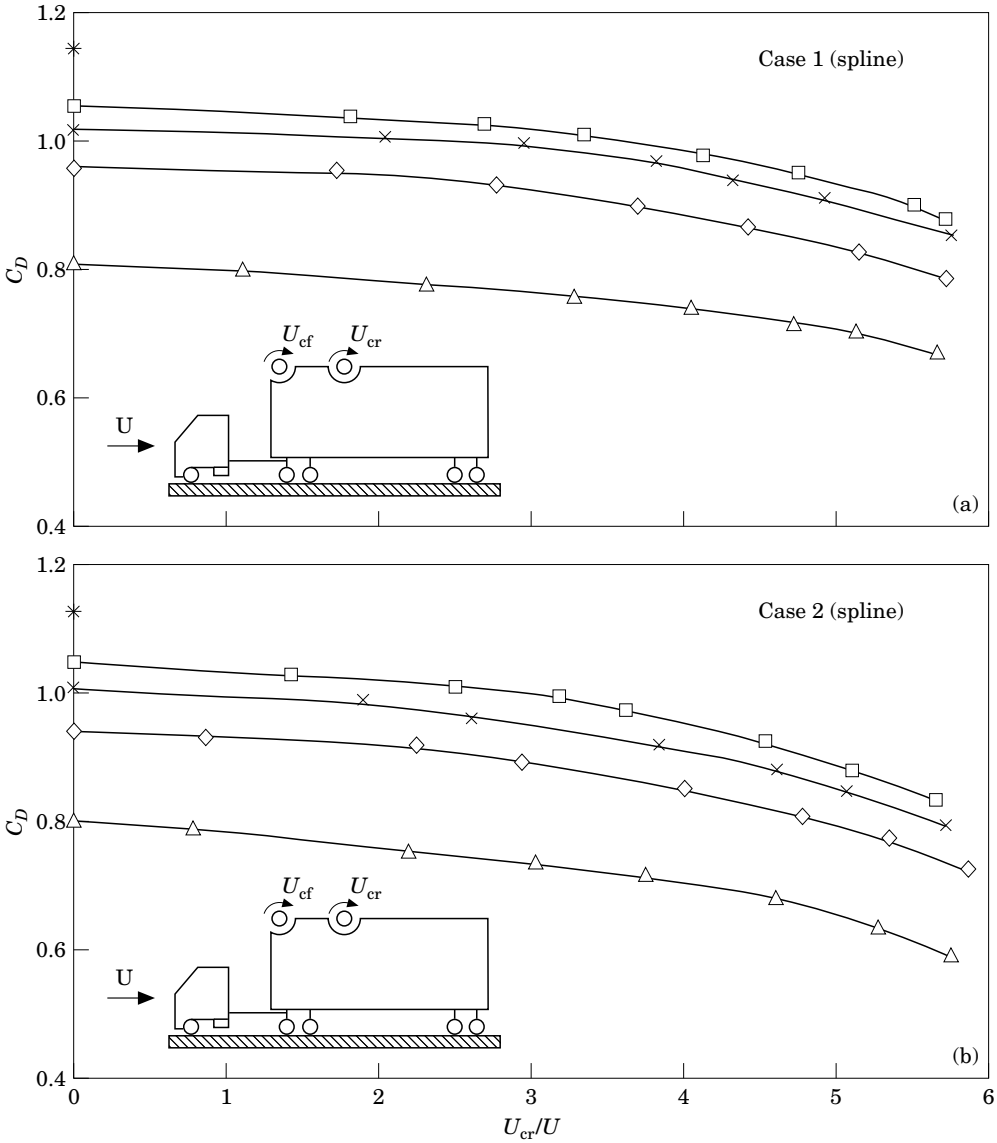

Figure 12. Variation of the drag coefficient C_D with the speed ratio for spline twin-cylinder configuration: (a) Case 1: both cylinders flush; (b) Case 2: front cylinder flush, rear cylinder raised 6·35 mm. $Re = 10^5$. (*) $U_{cf}/U = 0$; (⊟) $U_{cf}/U = 1{\cdot}4$; (⤫) $U_{cf}/U = 2{\cdot}7$; (⟐) $U_{cf}/U = 4{\cdot}1$; (△) $U_{cf}/U = 6{\cdot}1$.

(i) the surface singularity distribution with boundary-layer corrections;
(ii) the finite element integration of the Navier-Stokes equations.

It is important to recognize that numerical studies represent important contributions to the field. Numerical approach to multi-body systems with the moving surface boundary-layer control has received very little attention, and that too only recently. The fact that relatively simple numerical approaches can give excellent results using modest computational facilities (a personal computer or a work-station) is indeed significant. It is important to emphasize that numerical results, in general, substantiate the experimental and flow-visualization data. Furthermore, it should be pointed out

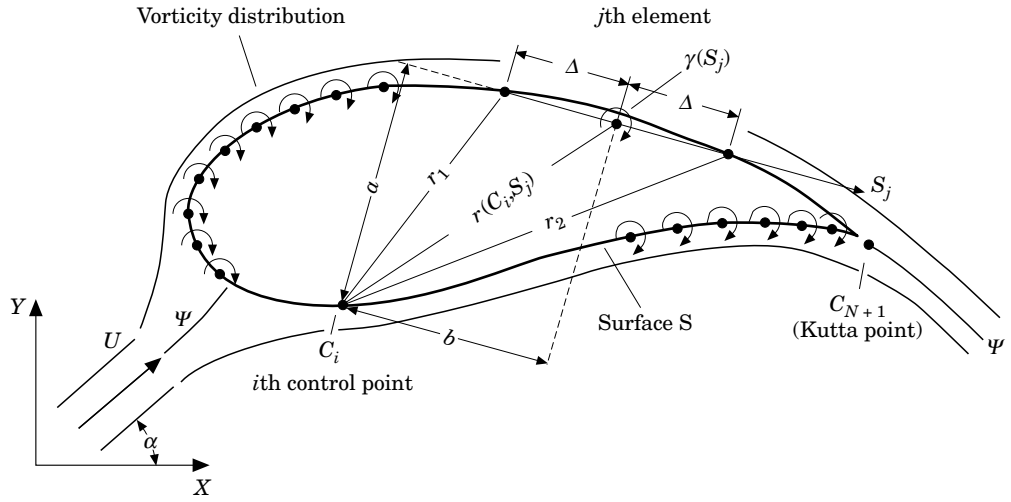

Figure 13. Singularity representation of the airfoil and notation for calculation of influence coefficients.

that comparison of numerical results with one's own wind tunnel and/or flow-visualization data is indeed scarce in the literature.

5.1. Surface Singularity Approach

The surface singularity procedure is described in detail by Mokhtarian (1988). It accounts for the wall confinement and involves replacement of the airfoil and wind tunnel walls with vorticity distribution γ in conjunction with appropriate constraint relations (Figure 13). Inclusion of a source within the contour of the airfoil models the wake when there is flow separation from the surface.

A finite difference boundary-layer scheme was used to introduce viscous corrections. It employs potential flow pressure-distribution results to calculate the boundary-layer characteristics at the top and bottom surfaces starting from the stagnation point until the point of separation.

The procedure used the displacement thickness to construct an equivalent airfoil and then iterate between the potential flow and boundary-layer scheme to converge to the final pressure distribution. Thus, the objective was to match the outer potential flow solution with the inner boundary-layer prediction. The thin shear layer approximations of the Navier-Stokes equations for steady, two-dimensional, incompressible flow were used. The finite difference method employed for viscous correction is due to Keller & Cebeci (1971, 1972). The eddy viscosity term was expressed as suggested by Cebeci & Smith (1974) which treats the turbulent boundary-layer as a composite layer consisting of inner and outer regions with separate expressions for eddy viscosity in each region. The details of the formulation and the finite difference procedure followed were those given by Cebeci & Bradshaw (1977), who have also discussed accuracy of the approach.

Typical results for the Joukowski airfoil with upper leading edge cylinder are presented in Figure 14. Wind-tunnel test results are also included to facilitate comparison. As the numerical approach is able to account for the wall-confinement effect, both sets of data are corrected for blockage. Considering the complex character of the flow, the correlation is indeed excellent and the results can be used with confidnece. Details of the numerical scheme are indicated in the flow chart (Figure 15).

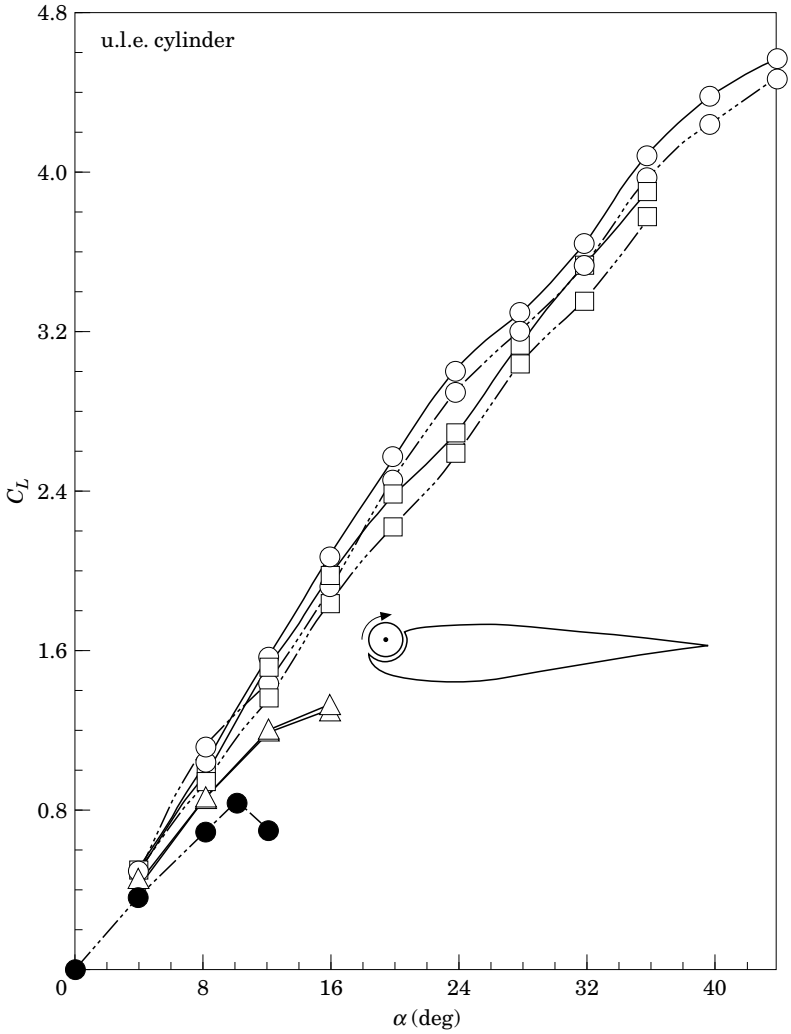

Figure 14. Variation of lift with angle of attack in presence of the MSBC as predicted by numerical and experimental procedures. Results account for blockage and end effects. Note that, in spite of the complex character of the flow, the correlation is excellent. (●) Base airfoil; (—) theoretical and (–···–) experimental results for: (△) $U_C/U = 1$; (□) $U_C/U = 3$; (○) $U_C/U = 4$.

Attempts were also made to apply the relatively simple panel method to this challenging problem of multi-element objects with momentum injection. During the past three decades, the classical panel method involving distribution of surface singularities has evolved to a sophisticated level where it can tackle complex geometries and flow-separation conditions. Maskew & Dvorak (1978) modelled separated flow by ''free-vortex lines'' having a known constant vorticity but initially of unknown shape. Successive iterations yield the converged wake shape. Ribaut (1983) accounted for the vorticity dispersion through dissipation and diffusion leading to a finite wake. The first-order panel method, employing linearly varying vorticity along each panel and incorporating dispersion in the wake to model the separated flow, is also attractive (Mukherjea & Bandyopadhyay 1990).

The panel descretization of the D-section as used by Munshi *et al.* (1995) is shown in

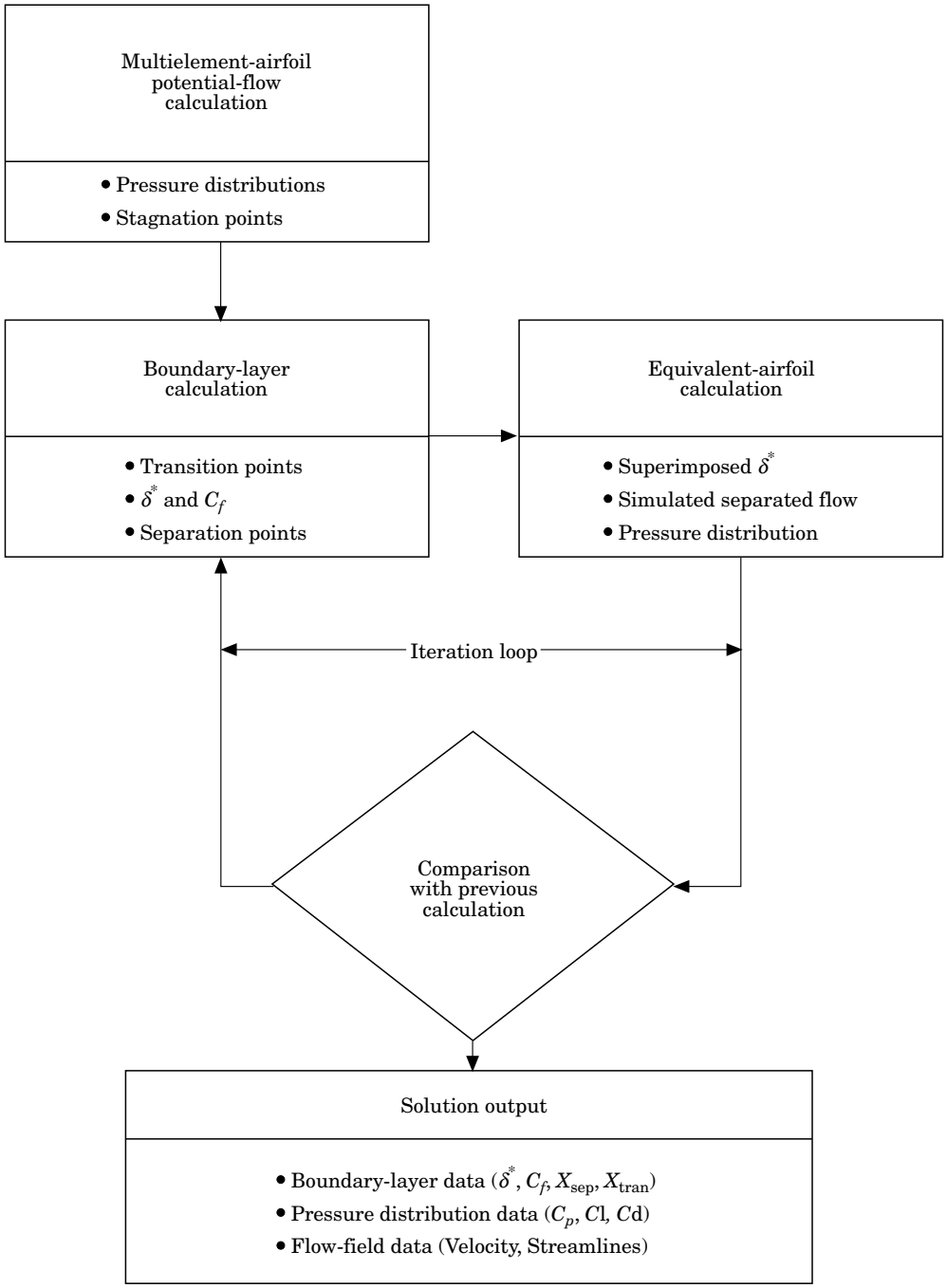

Figure 15. Flow chart for the numerical algorithm used to introduce viscous correlation in the surface singularity method: δ^*, boundary-layer displacement thickness; C_f, local skin friction coefficient, X_{sep}, downstream location of the separation.

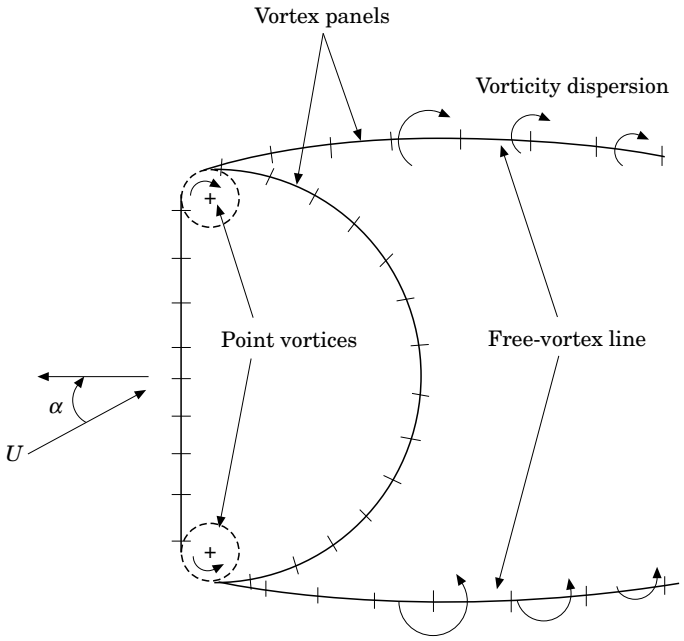

Figure 16. Schematic diagram showing a multi-element D-section with the moving surface boundary-layer control (MSBC) used in the present numerical study.

Figure 16. In the study, the momentum-injecting rotating cylinder was represented by a large number of panels (100–150). Each panel has a continuous distribution of linearly varying vorticity and a constant source strength. The separated flow was modelled by the ''free-vortex lines'' emanating from the lower and upper separation points. The free-vortex lines were also discretized into panels. At the beginning of the free-vortex line, the vorticity strength was taken to be equal to that at the separation point. The vorticity was allowed to dissipate at a given rate along the free-vortex lines resulting in a finite wake. An iterative scheme led to the final solution. Typically, 50–60 iteration cycles were required to achieve a convergence accuracy of about 10^{-6}.

The numerically obtained pressure distribution captures the suction peak on the rotating cylinder quite well (Figure 17). The numerical scheme also predicts a significant rise in the wake pressure, as confirmed by the experimental data. As shown in Figure 18, the drag coefficient predicted by the numerical scheme compares well with the experimental data even up to $\alpha = 30°$! The numerically obtained free-streamlines (Figure 19) show clearly that the wake becomes progressively narrower as the momentum injection is increased from $U_c/U = 0$ to $U_c/U = 4$.

5.2. Finite Element Navier-Stokes Solution

Here the stream-function-vorticity form of the Navier-Stokes equations was used in conjunction with the variable grid-size (~3000 nodes) finite element analysis as discussed by Modi & Yokomizo (1992) as well as Modi *et al.* (1994a). Such numerical solutions of multi-element airfoils and bluff bodies, with momentum injection, are indeed challenging and scarce. The parametric analysis involving a systematic variation of the speed ratio, angle of attack and the Reynolds number gave detailed information

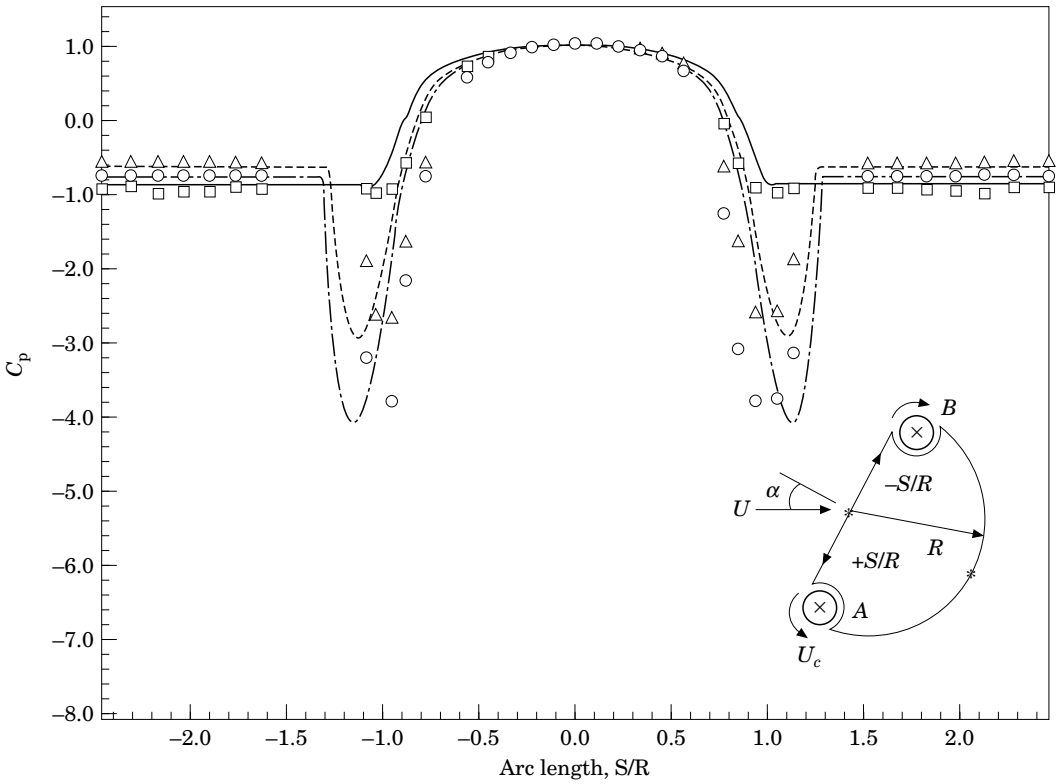

Figure 17. Typical surface pressure plots for the D-section showing effects of the momentum injection for Re = 66 000, $\alpha = 0°$. Similar plots were obtained over a range of the angles of attack. The panel code predicts the trends quite well even for such a complex flow field with momentum injection. Lines: theory; symbols: experiment. (—) $U_C/U = 0$; (□) $U_C/U = 0$; (- - - -) $U_C/U = 2$; (△) $U_C/U = 2$; (–·–·) $U_C/U = 4$; (○) $U_C/U = 4$.

about the pressure loading, separation condition and the time-dependent wake. It also showed, rather spectacularly, the effectiveness of the MSBC.

Figure 20 captures variation in the flow-field as the injected momentum is progressively increased through rotation of the cylinders from $U_c/U = 0$ to $U_c/U = 2$. The flow over the airfoil distinctly tends towards a potential character. The same trend can be observed through the spatial variation of the velocity vectors as shown in Figure 21 ($U_c/U = 4$).

6. FLOW VISUALIZATION

To get a better appreciation as to the physical character of the complex flow-field as affected by the angle of attack and momentum injection parameters, Modi *et al.* (1991e, 1994a, b, c, 1995) have also reported results of flow visualization studies. They gave useful information about the relative importance of the various system parameters, and hence assisted in the planning of the experiments as well as the numerical analyses. The flow visualization tests were carried out in a closed-circuit water channel facility (Figure 22). The models were constructed from Plexiglas and fitted with rotating cylinders driven by variable-speed d.c. motors. A suspension of fine polyvinyl chloride powder was used in conjunction with slit lighting to visualize

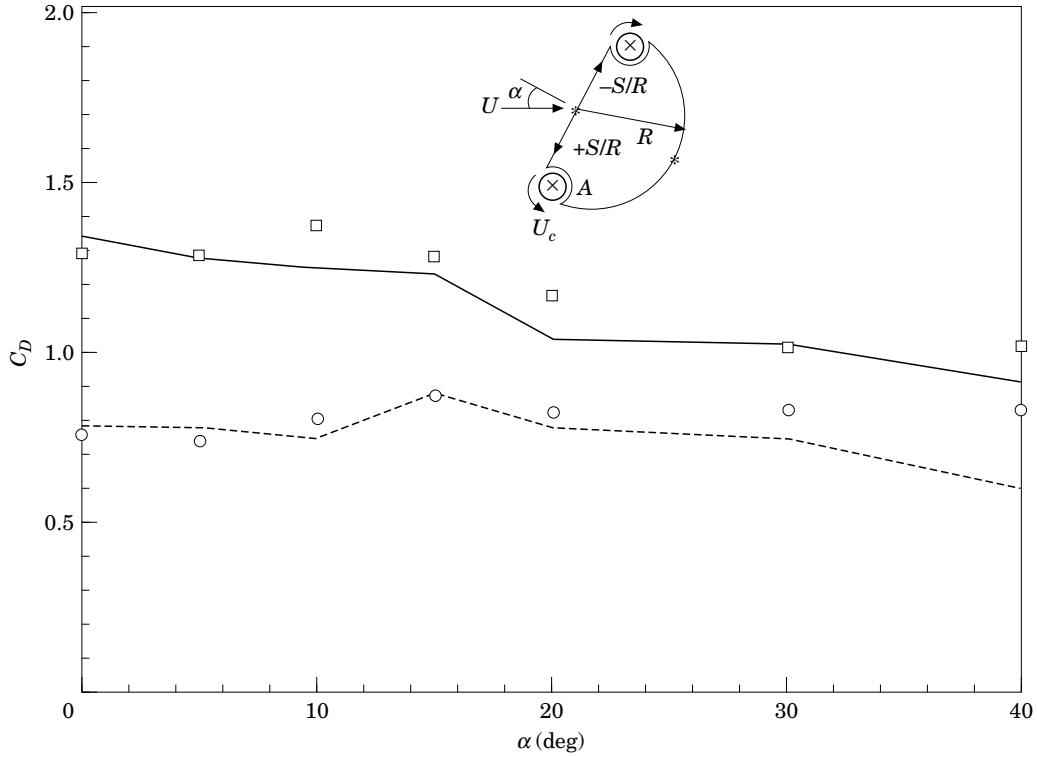

Figure 18. Comparison between numerical prediction and experimental measurement of the drag coefficient for the D-section in presence of momentum injection. Lines: numerical; symbols: experiment. (—) $U_C/U = 0$; (□) $U_C/U = 0$; (- - - -) $U_C/U = 4$; (○) $U_C/U = 4$.

streaklines. Both the angle of attack and cylinder speeds were systematically changed, and still photographs as well as video movies were taken. The Reynolds number was in the range 4×10^4–5×10^4.

The study showed, rather dramatically, the effectiveness of this form of boundary-layer control (Figure 23). With the leading-edge cylinder model at $\alpha = 20°$ and in the absence of cylinder rotation, a well defined early separation resulting in a wide wake is quite apparent, with large-scale vortices sweeping away downstream. However, with the cylinder rotating at $U_c/U = 4$, an essentially attached flow is established over most of the upper surface of the airfoil, even at such a high angle of attack, considerably beyond the nominal stall angle of around 10°.

At relatively lower rates of cylinder rotation, the flow character was found to be similar to that observed at $U_c/U = 1$, with the separation and reattachment regions progressively shifting downstream as the rotation rate increased. This is apparent through a progressive increase in U_c/U from 0 to 4. In fact, the flow pattern was found to be quite unsteady, with the vortex layer separating and forming a bubble on reattachment, the whole structure drifting downstream, diffusing, and regrouping at different scales of vorticity. Ultimately the flow sheds large- as well as small-scale vortices. This unsteady character of the separating shear-layer and the wake was clearly evident in the video. Thus the flow character indicated by the experimentally obtained time-averaged plots appears to be a fair description of the process.

Flow visualization results for a two-dimensional flat plate and a D-section cylinder, as presented in Figures 24 and 25, respectively, also tend to substantiate the

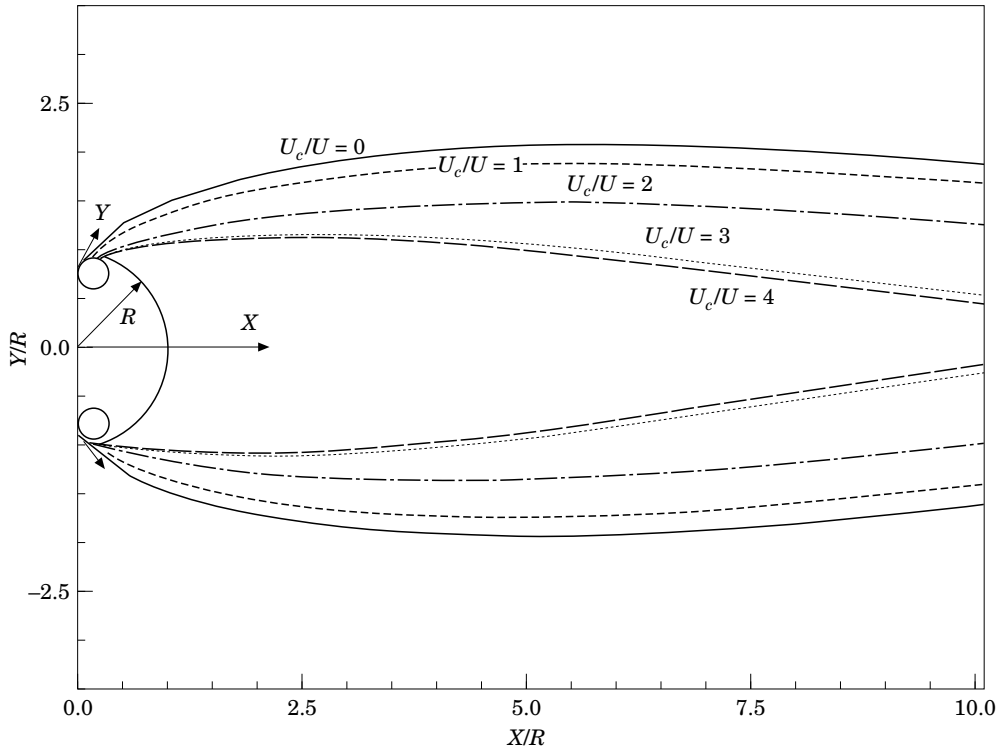

Figure 19. Narrowing of the wake, obtained numerically, suggesting reduction in the pressure drag of the D-section with momentum injection.

wind-tunnel data, which showed remarkable reductions in the drag coefficients. Furthermore, Figure 24 shows the effectiveness of the numerical finite element method mentioned earlier. Rectangular prisms show the same trend, thus establishing successful application of the MSBC procedure to diverse situations (Figure 26).

7. CONTROL OF WIND INDUCED INSTABILITIES

With the success of the moving surface boundary-layer control (MSBC) in increasing lift and reducing drag of both slender bodies at high angles of attack and bluff geometries, attention was directed towards control of wind-induced instabilities.

The response of aerodynamically bluff bodies when exposed to a fluid stream has been a subject of considerable study for quite some time. The prevention of aeroelastic vibrations of smokestacks, transmission lines, suspension bridges, tall buildings, etc. is of particular interest to engineers. Ever since the pioneering contribution by Strouhal, who correlated periodicity of vortex shedding with the diameter of a circular cylinder and velocity of the fluid stream, there has been a continuous flow of important contributions resulting in a vast body of literature. This has been reviewed rather adequately by Cermak (1975), Zdravkovich (1981), Welt (1988), Modi & Slater (1994), Munshi (1996) and others. In general, the oscillations may be induced by vortex resonance or geometric-fluid dynamic instability, called galloping.

Several passive devices, such as helical strakes, shrouds, slats, tuned mass and nutation dampers, etc. have been proposed over the years (Figure 27), and have exhibited a varying degree of success in minimizing the effects of vortex induced and

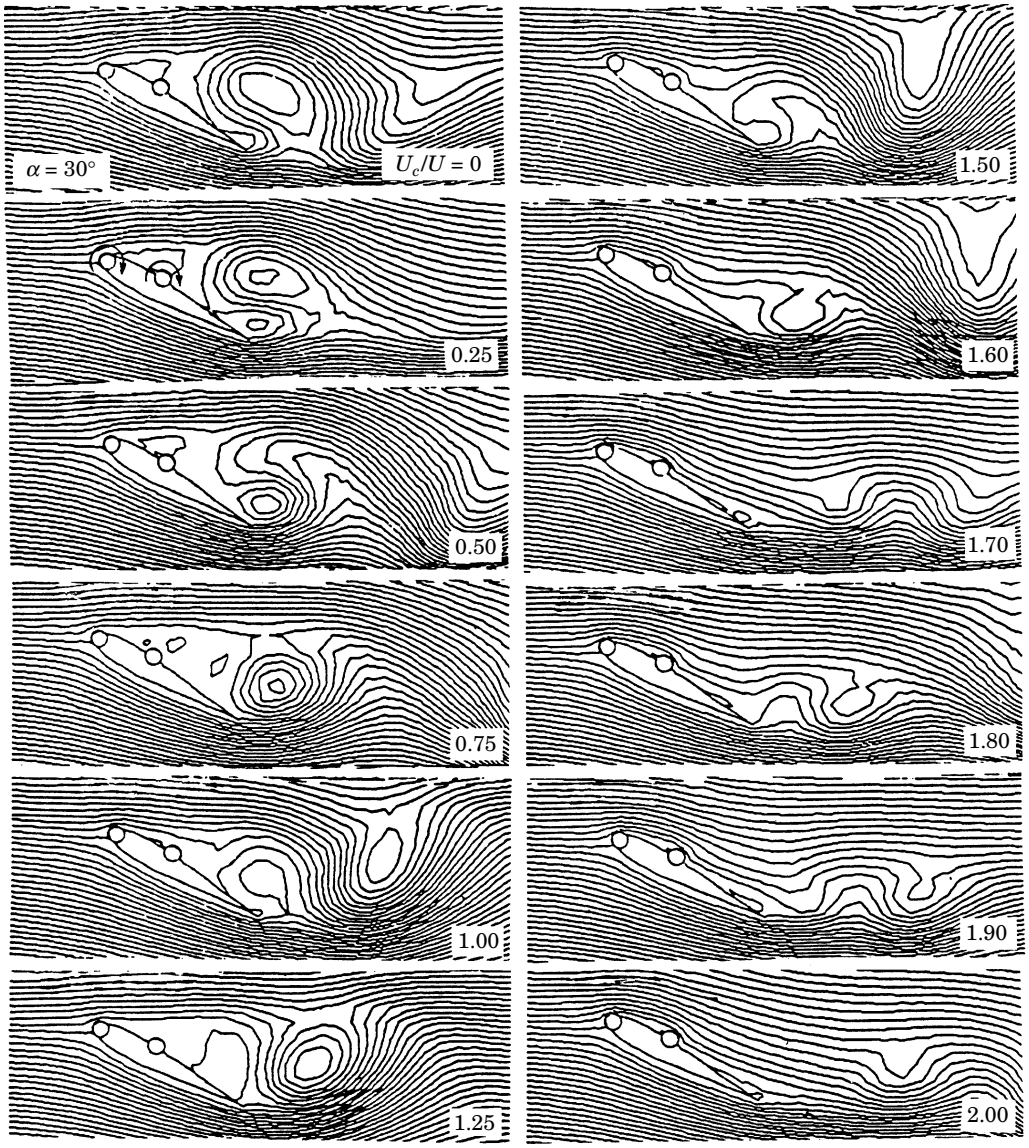

Figure 20. Variation in the flow-field as affected by progressive increase in the injected momentum. Note, the field tends to approach a potential flow in character. Flow visualization confirmed this behaviour. The streamlines were obtained using the finite element integration of the Navier-Stokes equations.

galloping types of instabilities (Zdravkovich 1984). In general, the vibration-suppressing devices tend to change aerodynamic characteristics of the structure in such a way as to interfere with and weaken the exciting force; while the dampers provide a mechanism for dissipating energy. It is of interest to note that all the above-mentioned procedures are passive in character. Semi-active devices such as a rotating element for the boundary-layer control and, through it, damping of the instabilities have received virtually no attention. Such an application of the MSBC was explored by Kubo *et al.* (1992, 1995), Munshi *et al.* (1996) and Modi *et al.* (1997) only recently.

Variation of the Strouhal number (S) with the Reynolds number (Re) for the flat

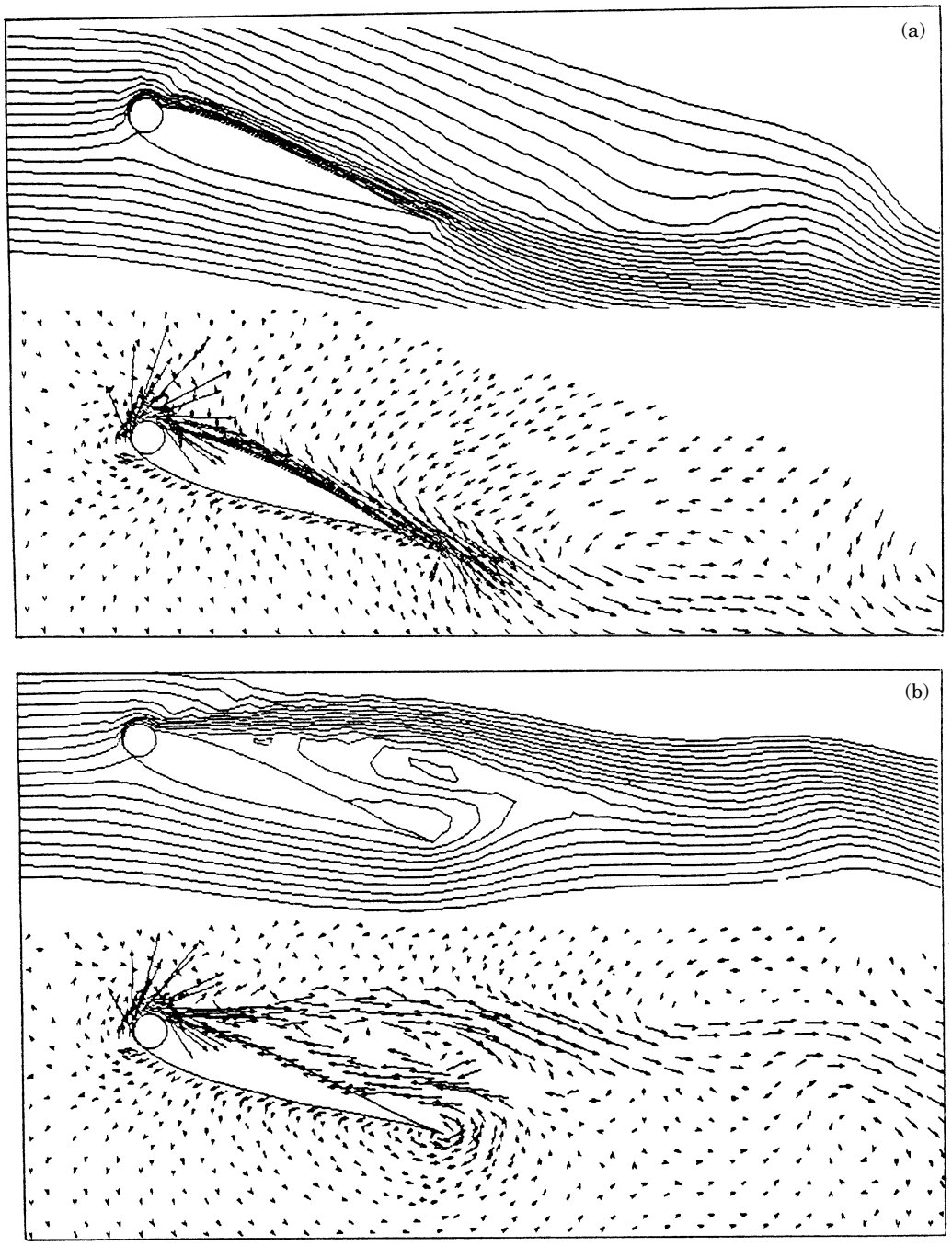

Figure 21. Fluid flow-field and velocity distribution as given by the numerical finite element study of a multi-element airfoil with momentum injection at $\alpha = 20°$. (a) $U_C/U = 4$; (b) $U_C/U = 0$.

plate with rounded tips due to the presence of cylinders, but in the absence of cylinder rotation, is shown in Figure 28(a). As expected, at a given Reynolds number S diminishes as the angle of attack increases. The effect of the cylinder rotation on the Strouhal number as a function of α for a fixed Re of 3×10^4 is presented in Figure

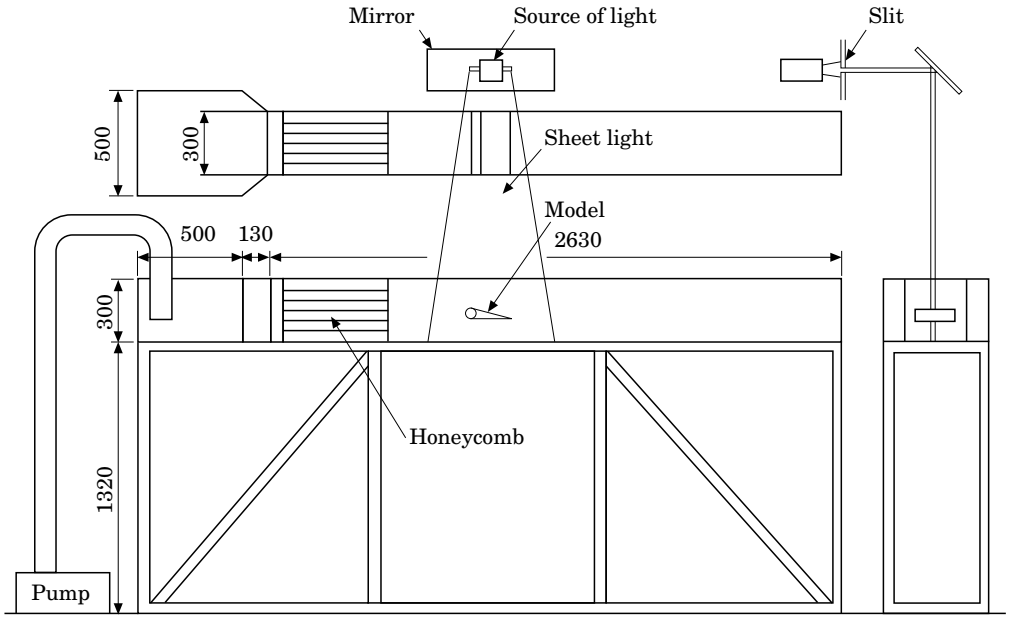

Figure 22. A schematic diagram of the closed circuit water tunnel facility used in the flow visualization study. Dimensions are in mm.

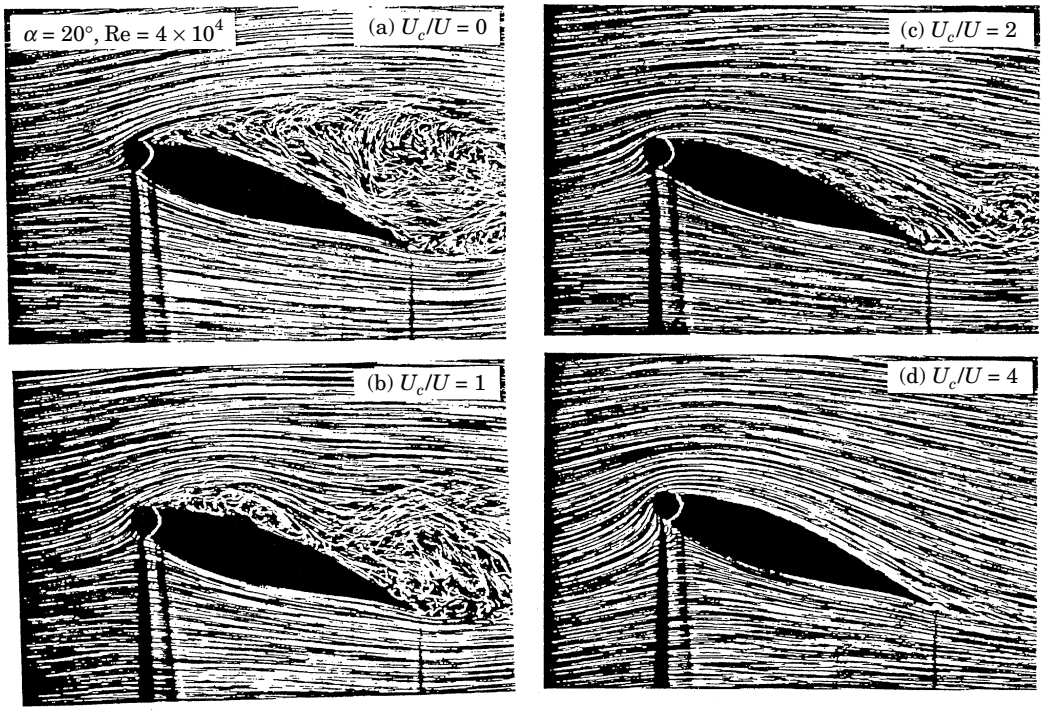

Figure 23. Typical flow visualization photographs showing the remarkable effectiveness of the moving surface boundary-layer control method. (a) Highly separated flow, at a high angle of attack, in the absence of the cylinder rotation; (b) appearance of a separation bubble, $U_C/U = 1$; (c) downward shift of the separation point with a distinct reduction in the wake width, $U_C/U = 2$; (d) essentially attached flow, $U_C/U = 4$.

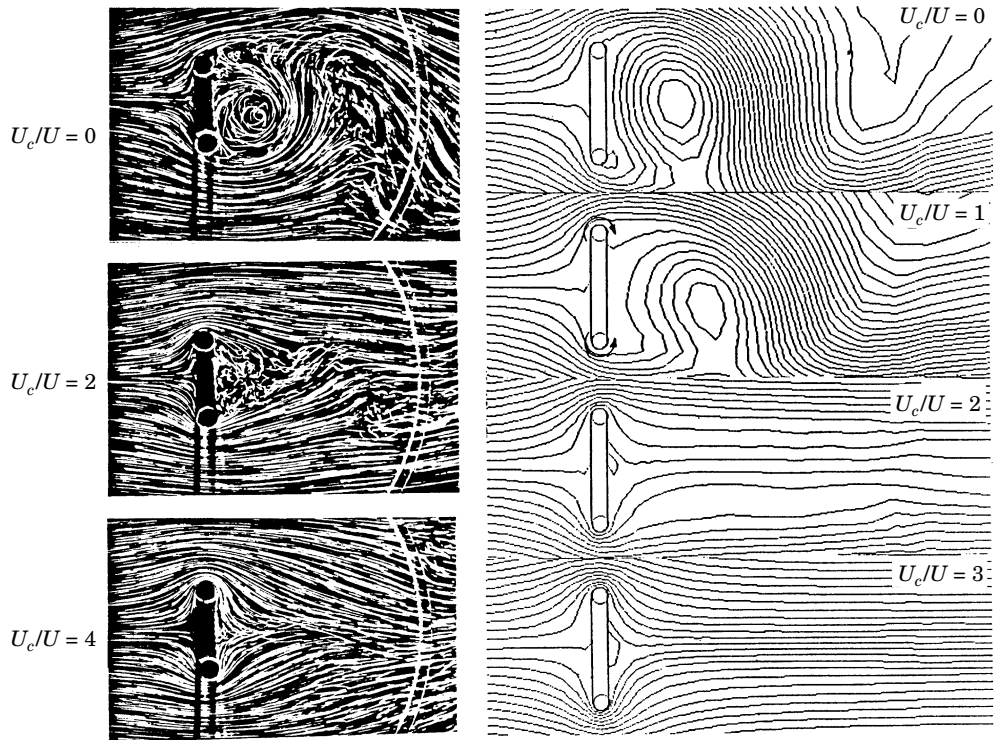

Figure 24. Typical flow visualization photographs for a flat plate at $\alpha = 90°$ showing the remarkable effectiveness of the moving surface boundary-layer control applied at the top and bottom edges. Numerical results using the finite element method are also presented for comparison.

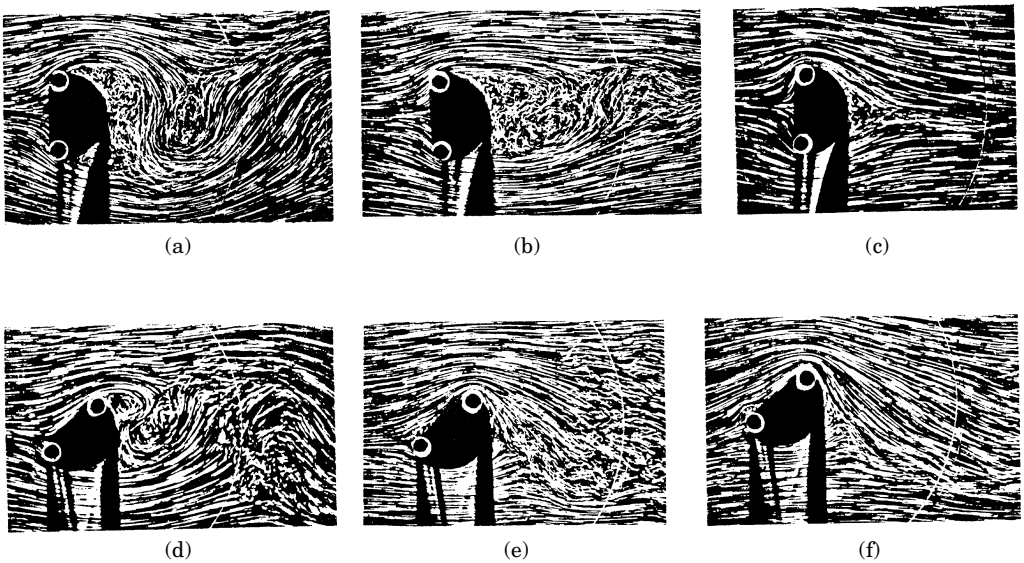

Figure 25. Flow visualization photographs showing effectiveness of the moving surface boundary-layer control (MSBC) as applied to the D-section. Note that at $U_C/U = 4$ the flow tends to approach a potential flow in character. (a) $\alpha = 0°$, $U_C/U = 0$; (b) $\alpha = 0°$, $U_C/U = 2$; (c) $\alpha = 0°$, $U_C/U = 4$; (d) $\alpha = 45°$, $U_C/U = 0$; (e) $\alpha = 45°$, $U_C/U = 2$; (f) $\alpha = 45°$, $U_C/U = 4$.

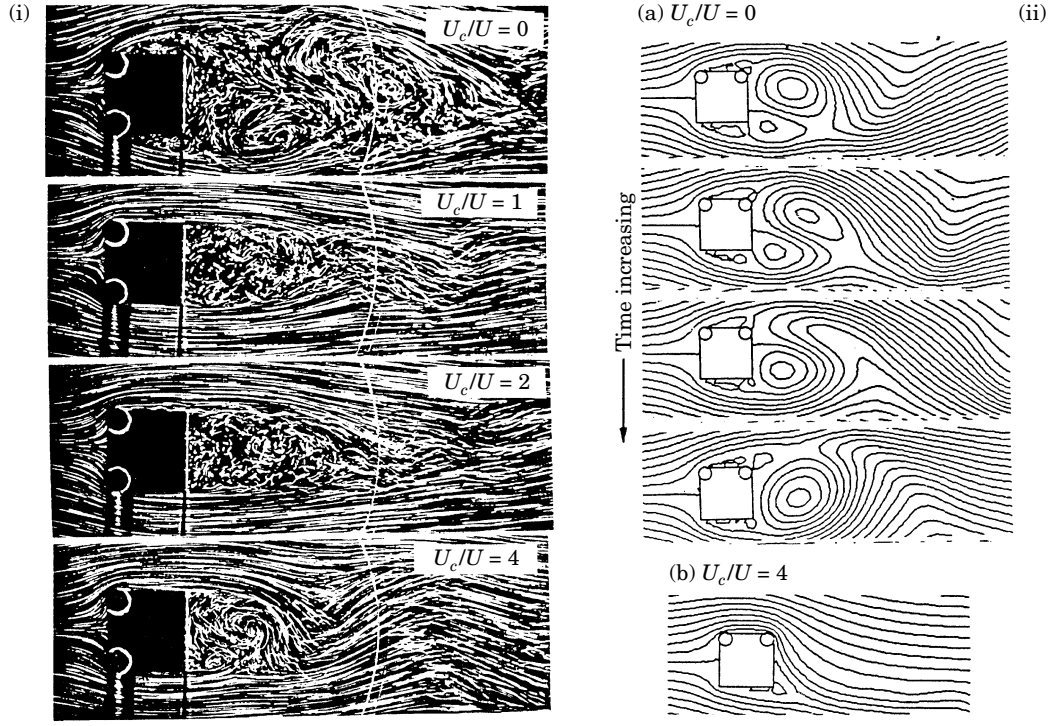

Figure 26. Typical flow visualization and finite element numerical studies with two-dimensional square prisms. (i) Flow visualization pictures showing effectiveness of the MSBC; reduction in the wake at $U_C/U = 4$ is rather spectacular, suggesting a significant decrease in the drag. Wind tunnel results showed it to be around 62%. (ii) Numerically obtained flow pattern showing progressive evolution of the wake for a square prism at $\alpha = 90°$.

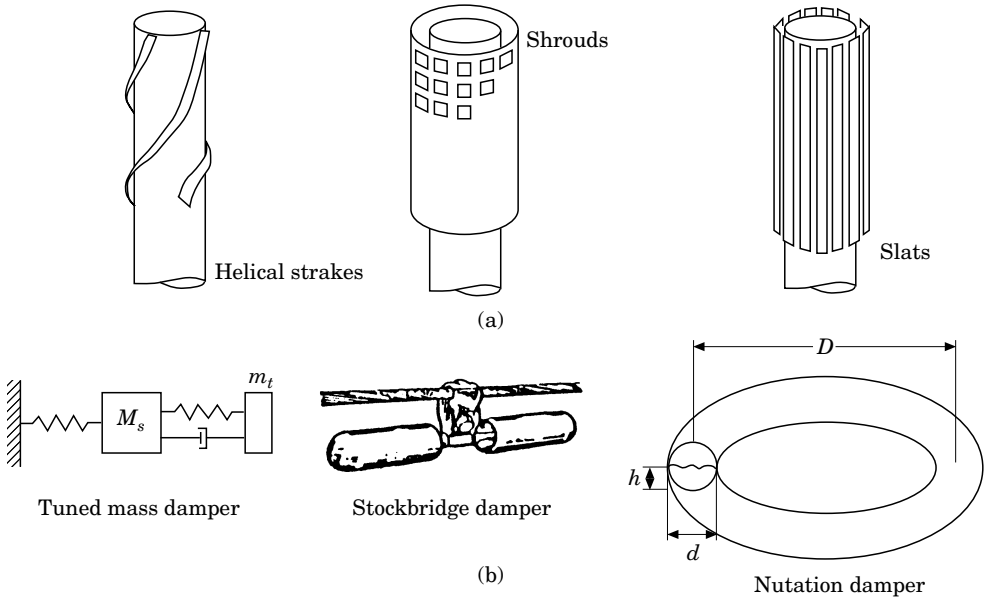

Figure 27. Passive devices used to control wind-induced instabilities. (a) Strakes, slats and shrouds modify system aerodynamics; (b) dampers provide energy dissipation mechanism.

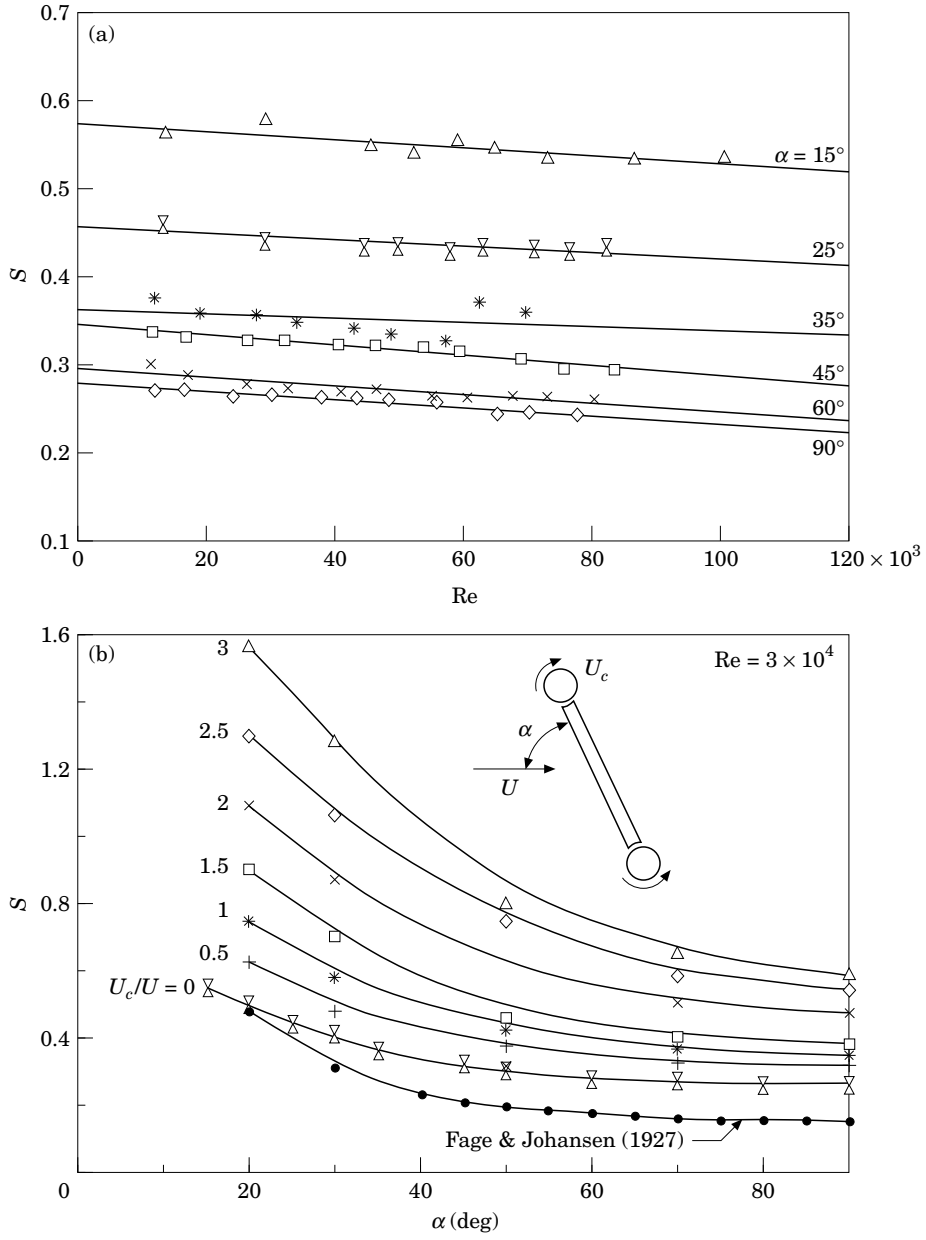

Figure 28. Strouhal number (S) associated with a flat plate having rounded edges due to tip cylinders; (a) variation with the Reynolds number and angle of attack in absence of cylinder rotation; (b) effect of momentum injection.

28(b). The classical results of Fage & Johansen (1927) are also included for comparison. A remarkable increase in the Strouhal number with cylinder rotation at a given angle of attack is apparent. It suggests an increase in the shedding frequency corresponding to narrowing of the wake. Thus the flat plate effectively projects reduced bluffness.

Kubo *et al.* (1992) applied the concept to a two-dimensional square prism provided with twin rotating elements at the corners of the front face (as well as several other configurations). The tests were carried out in a wind tunnel with the spring-supported model free to undergo plunging oscillations. The single cylinder rotation affected coherence of the vortex shedding, and hence suppressed resonant instability. On the other hand, twin-cylinder rotation successfully modified the loading to arrest the galloping. Excellent flow visualization pictures supported the wind tunnel test observations.

A study by Kubo *et al.* (1995) with a three-dimensional square prism lays a sound foundation for practical application of the concept to bridge decks, bridge towers and supertall buildings of the future (Figure 29). It clearly establishes that only a small section of the building is required to receive the MSBC for successfully arresting vortex resonance and galloping instabilities. This presents an entirely new area of exploration and applications. There are situations where ocean-based structures can also benefit from the concept.

After an uncertain beginning and interrupted advances over nine decades, it is

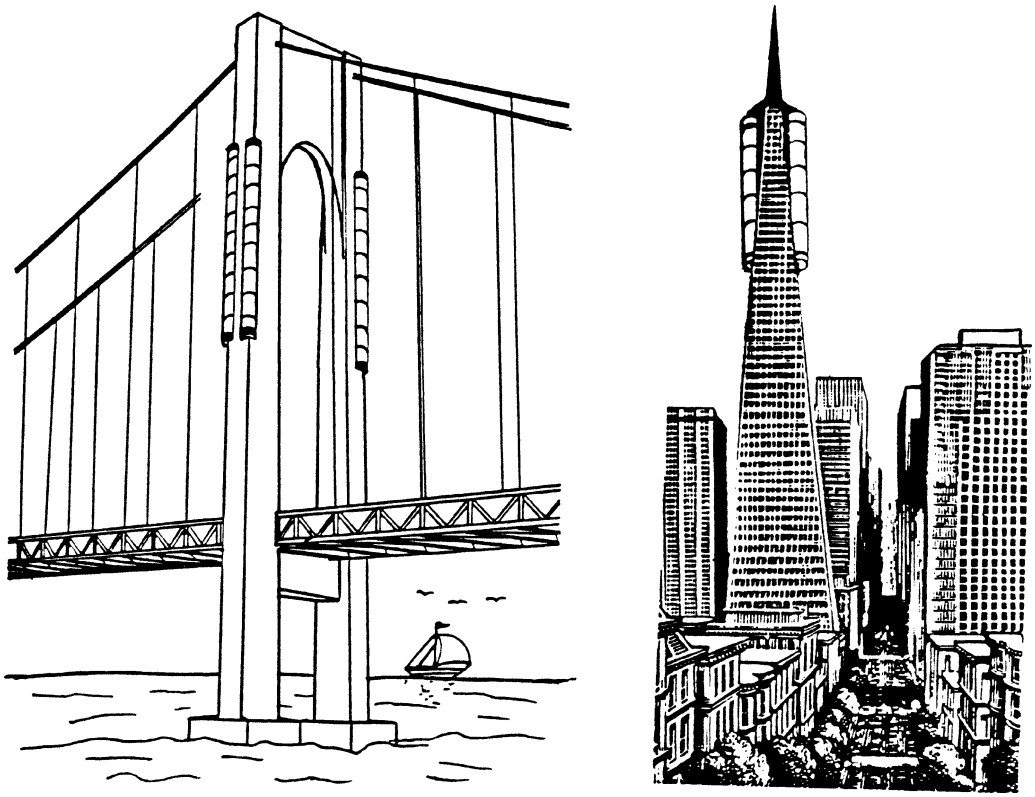

Figure 29. The MSBC concept presents an exciting possibility of application to the next generation of civil engineering structures such as bridge-towers and supertall buildings (Kubo *et al.* 1995).

apparent that the field presents considerable opportunity for further contributions. As the Gita puts it: "*Knowledge is merely a small island surrounded by a vast ocean of ignorance.*" No matter how far we advance, we will always be on the shores of that uncharted ocean. But then, one has to make a beginning, however humble it may be. After all, a journey fulfills itself in every step.

8. CONCLUDING REMARKS

Based on wind-tunnel tests, complemented by numerical and flow visualization studies reported in the literature, the following general comments can be made.

(i) Moving surface boundary-layer control (MSBC) can significantly increase lift, decrease drag and delay stall of aircraft. Its application to the next generation of high performance airplanes is indeed quite promising.

(ii) The concept is essentially semi-passive in character, requiring negligible amount of power for its implementation. This makes it quite attractive for real-life applications. During the reported wind tunnel tests with models, the peak power requirement is only around 90 W.

(iii) A numerical approach to the problem, even using a rather simple panel approach, can provide useful results of sufficient accuracy for a preliminary design. This is remarkable considering the highly complex character of the flow, and suggests significant savings in time, effort and computational cost.

(iv) The more elaborate finite element method is able to predict the character of the flow-field with considerable accuracy.

(v) Flow visualization study confirms the effectiveness of the MSBC quite dramatically.

(vi) The concept of the MSBC presents several avenues of promising applications. They include performance improvement of aircraft and their control surfaces; drag reduction of bus, truck and tractor-trailer configurations; suppression of vortex resonance and galloping type of wind-induced instabilities, particularly with reference to the next generation of light as well as long or high civil engineering structures, offshore platforms, etc.

ACKNOWLEDGEMENT

The preparation of this review was supported by the Natural Sciences and Engineering Council of Canada, Grant No. A-2181.

References

Alvarez-Calderon, A. & Arnold, F. R. 1961 A study of the aerodynamic characteristics of a high lift device based on rotating cylinder flap. *Technical Report RCF-I,* Stanford University, Palo Alto, U.S.A.

Associate Committee on Aerodynamics 1966 Report on the research co-ordination group on boundary layer control to suppress separation. National Research Council, Ottawa, Canada.

Bearman, P. W. 1980 Review of bluff body flows applicable to vehicle aerodynamics. *ASME Journal of Fluids Engineering* **102,** 265–274.

Betz, A. 1961 History of boundary layer control in Germany. In *Boundary Layer and Flow Control,* (ed. G. V. Lachmann), Vol. 1, pp. 1–20. New York: Pergamon Press.

Brooks, J. D. 1963 Effect of a rotating cylinder at the leading and trailing edges of a hydrofoil. *NAVWEPS Report 8042,* U.S. Naval Ordinance Test Station, U.S.A.

Brown, D. A. 1964 Peruvians study rotating-cylinder flap. *Aviation Week and Space Technology* **88,** 70–76.

CEBECI, T. & SMITH, A. M. O. 1974 *Analysis of Turbulent Flows,* 1st edn. New York: Academic Press.

CEBECI, T. & BRADSHAW, P. 1977 *Momentum Transfer in Boundary Layers,* 1st edn. Washington D.C.: Hemisphere-McGraw Hill.

CERMAK, J. E. 1975 Application of fluid mechanics to wind engineering. *ASME Journal of Fluids Engineering* **97,** 9–38.

CHANG, P. K. 1970 *Separation of Flow,* 1st. edn. New York: Pergamon Press.

CICHY, D. R., HARRIS, J. W. & MACKAY, J. K. 1972 Flight tests of a rotating cylinder flap on a North American Rockwell YOV-10A aircraft. NASA CR-2135.

COOK, W. L., MICKEY, D. M. & QUIGLEY, H. G. 1974 Aerodynamics of jet flap and rotating cylinder flap STOL concepts. Paper No. 10, AGARD Fluid Dynamics Panel Symposium on V/STOL aerodynamics, Delft, The Netherlands.

FAGE, A. & JOHANSEN, F. C. 1927 On the flow of Air behind an inclined flat plate of infinite span. *Proceedings of the Royal Society of London* A**116,** 170–197.

FAVRE, A. 1938 Contribution a l'étude expérimentale des mouvements hydrodynamiques à deux dimensions. Thesis presented to the University of Paris, France.

FLETTNER, A. 1925 The Flettner rotor ship. *Engineering* **19,** 117–120.

GOLDSTEIN, S. 1938 *The Modern Developments in Fluid Mechanics.* Oxford: O.U.P.

HOTZ, R. B. (editor-in-chief) 1971 Rotating cylinder flaps tested on OV-10A. *Aviation Week and Space Technology* **95,** cover page.

IVERSON, J. D. 1972 Correlation of Magnus force data for slender spinning cylinders. Paper No. 72-966, AIAA 2nd Atmospheric Flight Mechanics Conference, Palo Alto, U.S.A.

JOHNSON, W. S., TENNANT, J. S. & STAMPS, R. E. 1975 Leading edge rotating cylinder for boundary-layer control on lifting surfaces. *AIAA Journal of Hydronautics* **9,** 76–78.

KELLER, H. B. & CEBECI, T. 1971 Accurate numerical methods for boundary-layer flows; part 1: two-dimensional laminar flows. In *Proceedings of the Second International Conference on Numerical Methods in Fluid Dynamics,* New York, U.S.A.

KELLER, H. B. & CEBECI, T. 1972 Accurate numerical methods for boundary-layer flows; part 2: two-dimensional turbulent flows. *AIAA Journal* **10,** 1193–1199.

KRAMER, C. & GERHARDT, H. J. 1980 Road vehicle aerodynamics. In *Proceedings of the 4th Colloqiuim on Industrial Aerodynamics,* Aachen, Germany.

KUBO, Y., MODI, V. J., YASUDA, H. & KATO, K. 1992 On the suppression of aerodynamic instability through the moving surface boundary-layer control. *Journal of Wind Engineering and Industrial Aerodynamics* **41,** 205–216.

KUBO, Y., MODI, V. J., KOTSUBO, C., NAYASHIDA, K. & KATO, K. 1995 Suppression of wind-induced vibrations of tall structures through the moving surface boundary-layer control. *Journal of Wind Engineering and Industrial Aerodynamics* **61,** 181–194.

LACHMANN, G. V. 1961 *Boundary Layer and Flow Control.* New York: Pergamon Press.

MAGNUS, G. 1853 Über die Verdichtung der Gase an der oberflache glatter Köper. *Poggendorfs Annalen der Physik und Chemie* **88**, 604–610.

MASKEW, B. & DVORAK, F. A. 1978 The prediction of C_{Lmax} using a separated flow model. *Journal of American Helicopter Society* **23,** 2–8.

MODI, V. J. 1991 Moving surface boundary-layer control: experiments, analysis and applications. *The G.I. Taylor Memorial Lecture.* In *Proceedings of the 36th ISTAM Congress,* Indian Institute of Technology, Bombay, India.

MODI, V. J. & SLATER, J. E. 1994 Unsteady aerodynamics and vortex induced aeroelastic instability of a structural angle section. *ASME Journal of Vibration and Acoustics* **116,** 449–456.

MODI, V. J. & YOKOMIZO, T. 1992 On the boundary-layer control through momentum injection: numerical, flow visualization and experimental studies. In *Proceedings of the 6th International Symposium on Flow Visualization,* Yokohama, Japan.

MODI, V. J., SWINTON, P. G., MCMILLAN, K., LAKE, P., MULLINS, D. & AKUTSU, T. 1981 Moving surface boundary-layer control for aircraft operation at high incidence. *Journal of Aircraft* **18,** 963–968.

MODI, V. J., MOKHTARIAN, F., YOKOMIZO, T., OHTA, G. & OINUMA, T. 1987 Bound vortex boundary-layer control with application to V/STOL airplanes, In *Proceedings of the IUTAM Symposium on Fundamental Aspects of Vortex Motion,* Tokyo, Japan. Also in *Vortex Motion* (eds H. Hashimoto & T. Kambe), pp. 225–230; Amsterdam: North-Holland Publishing Company.

Modi, V. J., Mokhtarian, F. & Yokomizo, T. 1990 Effect of moving surfaces on the airfoil boundary-layer control. *Journal of Aircraft* **27,** 42–50.

Modi, V. J., Mokhtarian, F., Fernando, M. S. U. K. & Yokomizo, T. 1991a Moving surface boundary-layer control as applied to two-dimensional aerofoils. *Journal of Aircraft* **28,** 104–112.

Modi, V. J., Fernando, M. S. U. K. & Yokomizo, T. 1991b Moving surface boundary-layer control as applied to two and three dimensional bodies. *Journal of Wind Engineering and Industrial Aerodynamics* **38,** 83–92.

Modi, V. J., Fernando, M. S. U. K. & Yokomizo, T. 1991c Moving surface boundary-layer control: studies with buff bodies and application. *AIAA Journal* **29,** 1400–1406.

Modi, V. J., Ying, B. & Yokomizo, T. 1991d Boundary-layer control of buff bodies through momentum injection. *SAE Journal of Commercial Vehicles* **99,** 778–794.

Modi, V. J., Ying, B. & Yokomizo, T. 1991e An approach to design of the next generation of fuel efficient trucks through aerodynamic drag reduction. In *Proceedings of the ASME Winter Annual Meeting* (eds S. A. Velinsky *et al.*) Atlanta, U.S.A., Vol. DE 40, pp. 465–482.

Modi, V. J., Ying, B. & Yokomizo, T. 1992 Effect of momentum injection on the aerodynamics of several bluff bodies. *Journal of Wind Engineering and Industrial Aerodynamics* **41,** 713–714.

Modi, V. J., Munshi, S. R., Bandyopadhyay, G. & Yokomizo, T. 1994a On the moving surface boundary-layer control: a comparative study. In *Proceedings of the 3rd Asian Symposium on Flow Visualization,* Chiba, Japan.

Modi, V. J., Munshi, S. R., Bandyopadhyay, G. & Yokomizo, T. 1994b Multielement systems with moving surface boundary-layer control: analysis and validation. In *Proceedings of the 14th International Conference on Numerical Methods in Fluid Dynamics,* Bangalore, India.

Modi, V. J., Munshi, S. R., Mokhtarian, F., Bandyopadhyay, G. & Yokomizo, T. 1994c Multielement aerofoils with moving surface boundary-layer control: wind tunnel, numerical and flow visualization studies. In *Proceedings of the 19th Congress of the International Council of the Aeronautical Sciences,* Anaheim, U.S.A.

Modi, V. J., Munshi, S. R. & Yokomizo, T. 1995 Fluid dynamics of flat plates and rectangular prisms in the presence of moving surface boundary-layer control. In *Proceedings of the Ninth International Conference on Wind Engineering,* New Delhi, India.

Modi, V. J., Seto, M. L. & Munshi, S. R. 1997 On the dynamics and control of fluid-structure interaction instabilities. In *Proceedings of the Seventh International Offshore and Polar Engineering Conference,* Honolulu, Hawaii, U.S.A.

Mokhtarian, F. 1988 Fluid dynamics of airfoils with moving surface boundary-layer control. Ph.D. Thesis, The University of British Columbia, Vancouver, Canada.

Mokhtarian, F. & Modi, V. J. 1988 Fluid dynamics of airfoils with moving surface boundary-layer control. *Journal of Aircraft* **25,** 163–169.

Mokhtarian, F., Modi, V. J. & Yokomizo, T. 1988 Rotating air scoop as airfoil boundary-layer control. *Journal of Aircraft* **25,** 973–975.

Mukherjea, S. & Bandyopadhyay, G. 1990 Separated flow about a wedge. *The Aeronautical Journal of the Royal Aeronautical Society* **94,** 196–202.

Munshi, S. R. 1996 Aerodynamics of bluff bodies in presence of the moving surface boundary-layer control. Ph.D. Thesis, The University of British Columbia, Vancouver, Canada.

Munshi, S. R., Modi, V. J. & Yokomizo, T. 1995 Bluff body fluids dynamics of D-section with moving surface boundary-layer control. In *Proceedings of the Symposium on Flow-induced Vibration, ASME/JSME PVP Conference,* Honolulu, Hawaii, U.S.A.

Munshi, S. R., Modi, V. J. & Yokomizo, T. 1996 Effect of momentum injection on the drag reduction and flow-induced instabilities of a square prism. *International Journal of Offshore and Polar Engineering* **6,** 161–170.

Ribaut, M. 1983 A vortex sheet method for calculating separated two-dimensional flows. *AIAA Journal* **21,** 1079–1084.

Rosenhead, L. 1966 *Laminar Boundary Layers.* Oxford: O.U.P.

Schlichting, H. 1968 *Boundary Layer Theory,* 3rd edn. New York: McGraw-Hill.

Sovaran, G., Morel, T. & Mason Jr., T. W. 1978 Aerodynamic drag mechanisms of bluff bodies and road vehicles. In *Proceedings of the Symposium held at the General Motors Research Laboratory,* Warren, Michigan, U.S.A.

STEELE, B. N. & HARDING, M. H. 1970 The application of rotating cylinders to ship maneuvering. *Report No. 148*, National Physical Laboratory, Ship Division, U.K.

SWANSON, W. M. 1961 The Magnus effect: a summary of investigation to date. *ASME Journal of Basic Engineering* **83,** 461–470.

TENNANT, J. S. 1971 The theory of moving wall boundary-layer control and its experimental application to subsonic diffusers. Ph.D. dissertation, Clemson University, U.S.A.

TENNANT, J. S. 1973 A subsonic diffuser with moving walls for boundary-layer control. *AIAA Journal* **11,** 240–242.

TENNANT, J. S., JOHNSON, W. S. & KORTHAPALLI, A. 1976 Rotating cylinder for circulation control on an airfoil. *AIAA Journal of Hydronautics* **10,** 102–105.

TENNANT, J. S., JOHNSON, W. S. & KEATON, D. D. 1977 On the calculation of boundary-layers along rotating cylinders. *AIAA Journal of Hydronautics* **11,** 61–63.

TENNANT, J. S., JOHNSON, W. S. & KEATON, D. D. 1978 Boundary-layer flow from fixed to moving surfaces including gap effects. *AIAA Journal of Hydronautics* **12,** 81–84.

THWAITES, B. 1960 *Incompressible Aerodynamics,* 1st. edn., p. 215. New York: Dover Publications.

WACKER, T. A. 1985 Preliminary study of configuration effects on the drag of a tractor-trailer combination. M.A.Sc. Thesis, The University of British Columbia, Vancouver, Canada.

WEIBERG, J. A., GIULIANETTI, D., GAMBUCCI, B. & INNIS, R. C. 1973 Takeoff and landing performance and noise characteristics of a deflected STOL airplane with interconnected propellers and rotating cylinder flaps. NASA TM X-62, 320.

WELT, F. 1988 Study of nutation dampers with application to wind-induced oscillations. Ph.D. Thesis, The University of British Columbia, Vancouver, Canada.

YING, B. 1991 Boundary-layer control of bluff bodies with application to drag reduction of tractor-trailer truck congfiuration. M.A.Sc. Thesis, The University of British Columbia, Vancouver, Canada.

ZDRAVKOVICH, M. M. 1981 Review and classification of various aerodynamic and hydromechanic means for suppressing vortex shedding. *Journal of Wind Engineering and Industrial Aerodynamics.*

ZDRAVKOVICH, M. M. 1984 Reduction of effectiveness of means for suppressing wind induced oscillations. *Engineering Structures* **6,** 344–350.